FROM THE FIELD TO THE COMPUTER – A CASE STUDY ON THE DEVELOPMENT OF INPUT PARAMETERS FOR DEM SIMULATION PURPOSES

Michael E. Thompson

Conveyor Dynamics, Inc. (CDI)

ABSTRACT

Proper modelling of granular flow, particularly when it involves wet, sticky materials, is a common problem in chute design. A chute which easily handles dry granular material may become plugged when as little as 5% moisture by weight is added to the material mix. This study illustrates selected techniques for deriving more realistic estimates of the critical DEM input parameters required to properly model both dry and wet granular materials.

An additional goal was to devise test methods that could be applied to a easily shippable quantity of raw material (approx. 25 kg of material in a 20 litre bucket), and that could be simulated in a DEM program with a statistically relevant number of particles in a reasonable period of time, using a readily available computer hardware system, such as a desktop machine with 8 CPUs.

1. INTRODUCTION

DEM, or discrete element modeling is a computer simulation that provides estimates of the large scale flow behaviour of complex material systems, and is widely used in the design of bulk material transfer chutes, storage bins and hoppers.

Due to the extremely large number of particles involved in such simulations, computational time can be a time-consuming and expensive process. In order to keep the solution time and simulation costs down, the particles used in these simulations frequently do not include the full range of particle sizes present in the actual material. In fact, most simulations are performed by truncating the particle distribution at a certain minimum size, usually somewhere in the neighborhood of 15 mm to 25 mm.

Particles shapes can vary from almost spherical 'grains' or 'rounds' to almost flat 'slabs', and in many cases the differences in the particle shape can have a large effect on the angle of repose, or resting angle, of a pile of the material, whether that pile is a ground-supported stockpile or is an accumulation of material on a rock box or seam ledge inside the chute. Some DEM programs allow the user to select rounded or polyhedral shapes consistent with the observed shapes in the particle mix. Other DEM programs attempt to mimic the particle shapes by building conglomerations or clusters of spherical particles. Still simpler programs might subsume the particle shape influence into a rolling resistance parameter that is included as an input parameter in most DEM programs.

Cohesive forces between particles, and adhesive forces between particles and chute surface boundaries, are typically caused by liquid bridge forces if water or other liquid is present in the material, or by electrostatic van der Waal's forces if the material is dry. In the case of liquid bridge forces, this force is an insignificant fraction of the particle mass for particles much greater than 5–6 mm. The relevant particle size for electrostatic forces of significant magnitude is considerably smaller than this. Since the minimum particle size in a chute simulation is generally 3 to 4 times the particle size at which liquid bridge forces come into play, the DEM program must model these 'fines', where all the cohesive and adhesive action is occurring, as an equivalent set of larger (15–25 mm) particles.

This paper illustrates a combination of bulk material tests and DEM simulations to determine some of the critical input parameters required to perform a realistic DEM simulation involving a given material.

The material tested and simulated in this study is primary crushed zinc sulfide ore from a mine located in the Peruvian Andes. The mine provided one 20 litre bucket, containing a mix of approximately 25 kg of -50 mm particles, taken directly from the conveyor at the exit plane of the primary crusher discharge chute.

The DEM program used for the simulations is ROCKY DEM. Some of the parameters used in these simulations are unique to ROCKY, but most of them should be applicable to any DEM program.

2. DEM PARAMETERS

The following input parameters must generally be specified when setting up a flow simulation in ROCKY DEM, or in most other DEM programs:

- Particle size distribution – including minimum particle size
- Particle shape distribution
- Density and stiffness of any boundary surfaces
- Particle rolling resistance
- Particle density – often input as combination of bulk density and solid fraction
- Particle stiffness
- Boundary friction coefficients
  - Static and dynamic
- Internal (particle-to-particle) friction coefficients
  - Static and dynamic
- Adhesive distance
  - To allow for additional force factors, such as from liquid bridge forces, electrostatic forces, or even magnetic forces to act at a distance greater than the particle radius.

- Force fraction or stiffness fraction
  - The ratio of the adhesive force to the particle mass when using the constant adhesion model in ROCKY DEM
  - The ratio of the adhesive force to the particles stiffness when using the linear adhesion model in ROCKY DEM
- Coefficient of restitution ROCKY DEM nomenclature does not differentiate between 'adhesion', forces between dissimilar materials, and 'cohesion' forces between the same material. However, the program does allow the user to specify different adhesive distances and force or stiffness fractions between different material particles and boundary surfaces, and between different particulate materials combined into a single particle set. Throughout this paper, any adhesive interaction between similar particles will be referred to as 'cohesion'. Any interaction between particles with different properties, or between particles and boundary surfaces, will be referred to as 'adhesion'.

Many DEM programs and program manuals provide default values for many of these parameters. It is also customary practice in many cases to use approximate rule of thumb values for some of these parameters. This study is an effort to provide methods for reducing the number of default and rule of thumb values used in DEM simulations, and replace them with values derived from field and test data for the specific material being simulated.

NOTE: These tests are not exhaustive, and some parameter values must still rely on default or rule of thumb values.

3. TEST METHODS

The following test methods either provide a value for, or an estimate of, a required DEM parameter, or provides a benchmark that can be used to measure the accuracy of DEM simulations in the tests described. With such benchmarks, an iterative process can be used to fine tune the input parameters until the DEM model closely matches the actual test results.

3.1 PARTICLE SIZE DISTRIBUTION

For the purposes of ROCKY DEM calibration, the following system derived from a soil classification system used by MIT (Massachusetts Institute of Technology) was used.

Particle Classes and Sizes	
boulders	>150 mm
Large Cobbles	100 mm – 150 mm
Medium Cobbles	75 mm – 100 mm
Small Cobbles	50 mm – 75 mm
Large gravel	25 mm – 50 mm
Medium gravel	15 mm – 25 mm
Small gravel	6 mm – 15 mm
sand (rounded or lamellar)	70 μm – 6 mm
silt (rounded) or clay (lamellar)	< 70 μm

Table 3-1. DEM particle classes and sizes.

The relative quantity (% passing) for the particle classes and sizes in the +25 mm range were determined using photometric analysis of in situ material as it transited the conveyor system during a site inspection trip.

A representative sample of the same material, with the +50 mm particles removed, was collected during the site visit to the mine and sent for subsequent lab analysis. This material was passed through a set of sieves consisting of a 6 mm screen and a 70 μm screen to separate out the gravel fractions (-50 mm to +6 mm range) from the sand fraction (-6 mm to +70 μm) and the silt/clay fraction (-70 μm).

The gravel/cobble fraction (-50 mm to +6 mm) separated by the sieve process was hand sorted by size and weighed to determine the relative quantities of the large, medium, and small gravel fractions. These particles were then photographed for shape analysis, so that an appropriate combination of round or non-round shapes could be generated for the material calibration.

The sand and silt/clay fractions were weighed separately and subjected to microscopic analysis of the dominant shape. The microscopic particle shape analysis of these fractions allows for an estimated rolling resistance of the combined fines fraction. The principal reason for separating out the silt/clay fraction from the other fines is to determine the relative incidence of dust generation that might occur during transport of the dry material.

The sand and silt/clay fractions were later recombined for subsequent testing as the fines fraction.

3.2 PARTICLE DENSITY

Particle density was determined using a displaced water method. Several of the gravel particles were weighed and placed in a graduated cylinder. The cylinder was filled to a prescribed level with water, and the weight of the water was measured to determine the water's volume. The difference between the measured level and the actual water volume determines the volume occupied by the gravel particles. Particle density is then found by

$$\gamma_p = m_p/V_p$$

Where

γ_p = Particle Density
m_p = mass of particles
V_p = volume of particles

3.3 BULK DENSITY

The bulk density of the complete -50 mm sample (combined gravel and fines fractions) was measured prior to the sieving operation. A container with a known volume and tare weight was filled with the sample material and the net weight of the material was measured. After the sieving operation, the sand and silt/clay fractions were recombined as a fines fraction, and the bulk density of the fines fraction was determined by the same method. The calculation is similar to that for the particle density, except

$$\gamma_b = m_b/V_b$$

Where

γ_b = Bulk Density
m_b = net mass of material in container
V_b = volume of container

3.4 MOISTURE CONTENT

The moisture content of the fines fraction was determined by drying three different 20 gram samples in a Mettler LJ16 moisture analyser, and comparing the wet weight to the dry weight. Percent moisture is calculated and reported on a 'dry weight' basis:

% moisture = (wet weight – dry weight) x 100/(dry weight)

NOTE: This result is the percentage moisture of the fines fraction only. The percentage moisture for a representative sample of the entire particle collection would be significantly lower due to the increased dry weight mass of the combination of the larger particle fractions and the fines fraction.

While moisture content is not a programmable parameter for the ROCKY DEM program, it is an important measurement, as the moisture content of the material can make radical changes in the behaviour of the bulk material.

3.5 ANGLE OF REPOSE

Angles of repose were measured on a material testing rig, which incorporates a cylindrical test cell with an I.D. of 145 mm and a height of 95 mm. The test cell is filled level with material and the cylinder is lifted using a screw-jack mechanism at the rate of approximately 2 mm/s. Once the cylinder is well clear of the resulting conical or cylindrical pile, an angle gauge is used to measure the resulting angle of repose.

This test was performed on the -50 mm sample prior to the sieving operation, and repeated for the -6 mm fines fraction after sieving, and again after the material was dried. The AoR of the -50 mm to +6 mm gravel fraction was also measured after sieving and drying. A photographic record of each test was made.

The results of this test are used in combination with a DEM simulation of this test to confirm that the simulated material has the same angle of repose as the real material.

3.6 SURCHARGE ANGLE

Once the angle of repose test has been completed, the pile is subjected to a series of vibrations using an elliptical offset vibrator attached to the test rig's table. These vibrations mimic the settling action that occurs due to material trampling as it transits the idler sets along the length of a conveyor belt. The surcharge angles are measured and photographed in the same way as the angle of repose.

The results of this test can be used to determine required material profiles on the feed conveyors in a chute simulation.

3.7 COMPRESSIBILITY

Material compressibility is measured using unconfined compressive strength (UCS) and confined compressive strength (CCS) methods developed by CDI. Both these tests measure uniaxial stresses and strains in the material.

> **UCS** – For the UCS test, un-compacted material is formed into a pile using the same methodology as for the angle of repose test. This pile is subjected to a series of loads using a pressure plate equipped with a load sensor and a position indicator. The load is applied normal to the test table surface, and the pressure plate position after each load application is recorded. The material is free to move horizontally, in the same way it would be able to move during an impact on a chute flow control surface.
>
> **CCS** – For the CCS test, un-compacted material is loaded into a test cell with an I.D. of 145 mm and a height of 95 mm. The test cell walls eliminate any material strain in the horizontal direction, and also tend to prevent the escape of air from the void spaces between the particles. The material in the test cell is subjected to a series of loads using a pressure plate equipped with a load sensor and a position indicator. The load is applied normal to the test table surface, and the pressure plate position after each load application is recorded.

3.8 MATERIAL STIFFNESS

Material stiffness's are derived from the stress-strain data collected during the compressibility measurements. This data is used to determine the order of magnitude of the material stress to use in the DEM simulation. In the DEM particle impact algorithm, the particle stiffness plays a critical role in determining the energy dissipation due to the inelastic collisions. During the UCS and CCS compression tests, the stiffness measured is for the bulk material, and to properly calibrate the DEM model, this data is used to estimate of the stiffness of the individual particles included in the DEM simulation.

CCS Expansion - In addition to the CCS compression test, a CCS expansion test is performed to estimate the actual particle stiffness without the influence of moisture. A high load is applied to the dried material and the load is slowly released. The amount of expansion is measured as the force decreases. The high initial loading insures that the particles in the material are making good contact, so that the stiffness measured this way maintains a fairly constant value over the range of consolidation stresses.

3.9 FRICTION COEFFICIENTS

Particle-to-Wall Friction Coefficients
Friction coefficients are determined using a tilt table method. After each applied load during the CCS test, the test table surface is tilted until the test cell slides along the resulting slope. The static friction coefficient is determined by the angle at which the sliding motion commences. The dynamic friction factor is determined by the table angle and the acceleration time for the moving test cell to measure a predetermined distance at the static friction angle.

For this particular series of tests, the table surface was clean carbon steel. The same test can be performed on a variety of surfaces, including other types of steel, ceramic tile materials, or high-density plastic materials.

Particle-to-Particle Friction Coefficients
This test is similar to the particle-to-wall tests, but a fixed test cell is attached to the tilt table, and a mobile test cell is stacked on top of the fixed test cell. Both test cells are filled with un-compacted material, and loads are applied as for the CCS test. The static and dynamic friction factors are determined in the same manner as for the particle-to-wall test.

4. TEST RESULTS

4.1 PARTICLE SIZE DISTRIBUTION AND PARTICLE SHAPES

4.1.1 Particle Sizes

Using a combination of photometric and sieve analysis, the particle size distribution for the primary crushed zinc sulfide ore to be as shown in Table 4-1 was determined.

Particle Size Distribution			
Particle Class	**Size**	**% by Mass**	**% Passing**
boulders	150 mm -200 mm	4.9	100
Large cobbles	100 mm – 150 mm	10.1	95.1
Medium cobbles	75 mm – 100 mm	7.9	85.0
Small cobbles	50 mm – 75 mm	3.4	77.0
Large gravel	25 mm – 50 mm	3.9	73.6
Medium gravel	15 mm – 25 mm	15.7	70.0
Small gravel	6 mm – 15 mm	16.8	54.1
sand (rounded or lamellar)	70 μm – 6 mm	35.5	37.4
silt (rounded) or clay (lamellar)	< 70 μm	1.8	1.8

Table 4-1. Particle size distribution.

Figure 4-1. In situ material for photometric analysis.

Figure 4-1 shows the photo of the in situ material used to determine the relative distribution of the +25 mm particles. The distance between the idler sets on either side of the belt was used as a basis for determining the particle sizes, and for calculating the skew correction required due to the angle of the visual field.

This photo is a still image captured from a video of the belt while running. This particular frame had the best angle for determining the particle sizes, but variable surge loading of the belt resulted in a reduced material cross-section in this view, with fewer visible cobbles and boulders. Based on this photo, the material mass included in the original particle count was about 67 kg, whereas the conveyor design load of 1 500 t/hr, coupled with the belt speed of 4.2 m/s, would produce a mass of 99 kg for the 1 m long section of belt between the idler frames in this photo. Because of the observed deficit in total mass, and the lack of large particles in particular, the particle size distribution was adjusted by adding additional boulder and cobble sized particles to the calculations to bring the total mass included in the particle size analysis to 99 kg.

4.1.2 Particle Shapes of Gravel Fractions

Figure 4-2, Figure 4-3 and Figure 4-4 show the shapes of the -50 mm to +6 mm gravel particles included in the sample sent to CDI's lab for analysis. These photos were used to select appropriate polygonal shapes for the non-round particles included in the DEM Calibration model.

Figure 4-2. -50 mm to +25 mm from sample.

Figure 4-3. -25 mm to +15 mm from sample.

Figure 4-4. -15 mm to +6 mm from sample.

Figure 4-5 shows a selection of the -6 mm fines. Analysis of this photo indicates that the smallest particles observed for the material in the sample were about 0.2 mm in diameter. Many of the particles included here are conglomerations of smaller particles.

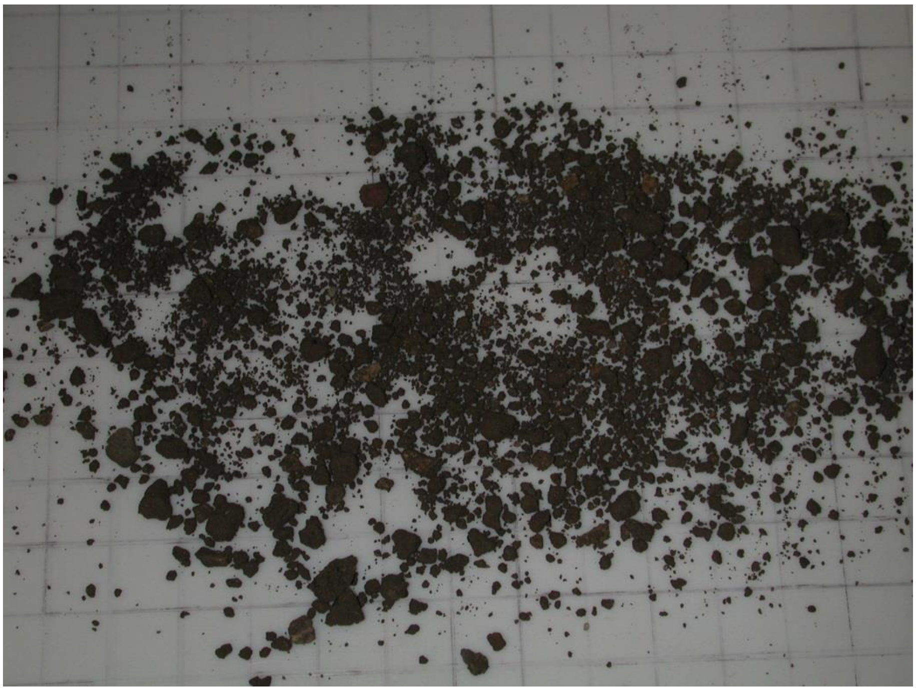

Figure 4-5. -6 mm fines from sample.

4.1.3 Particle Shapes of Fines Fractions

A micro-photographic examination of the wet fines is shown in Figure 4-6. The screen in the background has a 70 μm mesh. The smallest particles seen here are about 2 meshes, or 0.14 mm in diameter, which is consistent with the 0.2 mm size observed in Figure 4-5. The larger gravel particles show evidence of agglomerated fines clinging to them, and many of the larger particles are conglomerates composed of multiple smaller particles.

Figure 4-6. Micro-photo of wet fines.

Figure 4-7 shows a similar micro-photo of the -6 mm to +70 μm sand fraction taken after the material was dried and resieved. Figure 4-8 shows the -70 μm silt/clay fraction, with no background mesh.

Figure 4-7. Micro-photo of dry sand.

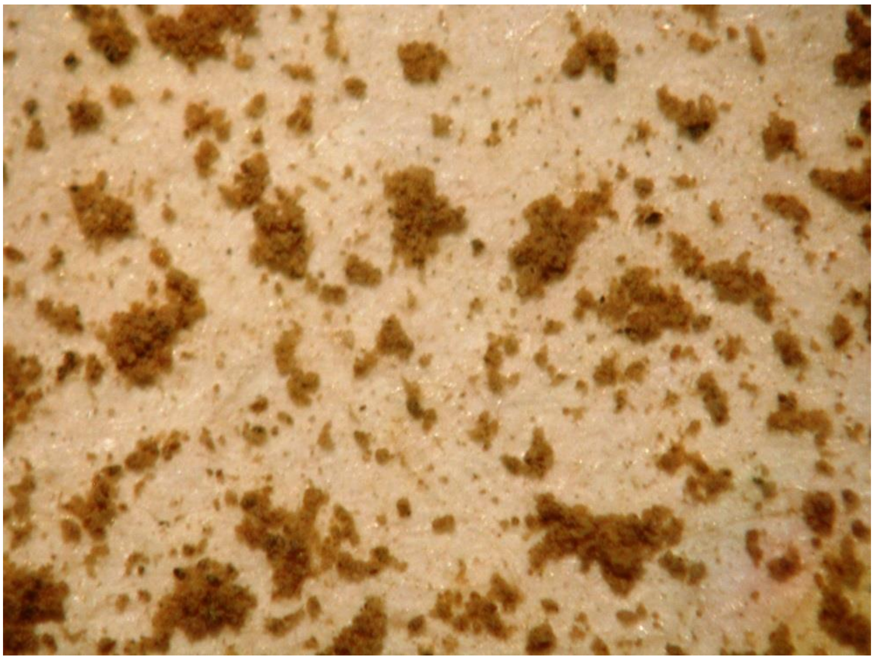

Figure 4-8 Micro-photo of dry silt/clay.

The angular characteristic of the various fines fractions indicates that they will not roll well. Since these particles would be simulated using round particles, it is necessary to adjust the rolling resistance factor to achieve a realistic angle of repose in the DEM simulation.

4.2 MATERIAL DENSITY AND MOISTURE CONTENT

Particle density measured in lab	2750	kg/m^3
Bulk density reported by the mine	1800	kg/m^3
Bulk density of -50 mm sample, Wet	1663	kg/m^3
Bulk density of -50 mm sample, Dry	1900	kg/m^3
Bulk density of -50 mm to +6mm gravels	1603	kg/m^3
Bulk density of -6 mm fines, Wet	1146	kg/m^3
Bulk density of -6 mm fines, Dry	1601	kg/m^3
Moisture content of fines	5.4	%

Table 4-2. Material density and moisture content.

Bulk density reported here is for un-compacted samples of the various material fractions tested. The variation in bulk density with consolidation stress is given later in Section 4. The bulk density of the various dry fractions are higher than for the same material wet due to the fact that the dry fines are not agglomerated into larger particles, and the smaller dry particles can pack closer together, and fill smaller voids between the gravel particles in the -50 mm sample.

Given that the -50 mm sample does not include the larger cobbles and boulders included in the primary crusher output, the densities measured in the laboratory are consistent with the 1 800 kg/m^3 bulk density reported by the mine. However, the fact that wet materials tested have significantly lower bulk densities than the equivalent dry materials means that the material expands when wet, and any chute designed to handle the wet material should use a volumetric flow rate based on a bulk density of approximately 1 600 kg/m^3.

Moisture content of the fines fraction is calculated on a dry basis. Gravel and cobble fractions of the material sample appeared to be drier than the fines, and the actual moisture content of the bulk material on site when the sample was collected was probably less than 5%.

4.3 ANGLE OF REPOSE (AoR)

There is often some asymmetry in the pile produced by the angle of repose test. Angle measurements are generally made on the left and right side of the pile, separated by about 180 degrees. Additional measurements may be made at other locations if there is a significant deviation in one area of the pile.

Figure 4-9 shows the AoR of the material including the gravel fractions from the sample delivered to the lab. This photo clearly shows that the combination of the angular gravel fractions and the wet fines fractions can sustain a vertical face, even with no compressive force applied to the pile. From this perspective the pile appears quite symmetrical on the left and right sides.

Figure 4-10 shows the front edge of the same pile as seen from the side. The rear edge showed the same 90 degree AoR as the left and right sides. Inspection showed that the front side of the pile contained relatively more fines and fewer large gravel particles. This indicates that the angular gravel fractions play a significant role in binding the bulk material into a cohesive mass that can create material bridges resulting in chute blockages. An accurate DEM simulation should therefore include reasonably accurate models of these gravels as polyhedral non-round particles.

Figure 4-9. AoR of wet -50 mm sample – left side.

Figure 4-10. AoR of wet -50 mm sample – front side.

Figure 4-11 and 2 shows the AoR of the -6 mm fines fraction at different levels of moisture content.

Figure 4-11. AoR of wet -6 mm fines – left side.

Figure 4-12. AoR of dry -6 mm fines – right side.

An angle of repose test was also performed for the -50 mm to +6 mm fraction after it had been sieved and dried. The result is shown in Figure 4-13.

Figure 4-13. AoR of dry -50 mm to +6 mm gravel – left side.

The dried gravels and fines were recombined and Figure 4-14 shows the angle of repose for the -50 mm dry sample.

Figure 4-14. AoR ofdry -50 mm sample.

Table 4-3 gives a summary of the results of the AoR tests.

Material	AoR Left	AoR Right	AoR Front
	[deg]	[deg]	[deg]
-50 mm sample - Wet	90	90	32
-50 mm sample – Dry	31	28	-
-50 mm to +6mm gravel - Dry	39	45	-
-6 mm fines – Wet	38	42	-
-6 mm fines - Dry	38	38	-

Table 4-3. Summary of AoR results.

These piles show that the fines alone cannot achieve the same bridging effect observed when both the gravel and fines fractions are present.

The dry -50 mm sample shows a pronounced dihedral angle. The top portion of the pile is resting at between 57^o (left) and 45^o (right) due to internal support from gravel particles buried inside the fines, showing that there is some potential for bridging even when the material is dry.

A comparison of the wet and dry AoR for the fines fraction is used to determine the rolling resistance and the cohesive force factors required for the 25 mm DEM particles used to model the bulk fines. Here the similarity of the AoR for the fines and the gravel indicate that the 25 mm round particles used to simulate the fines will require a relatively higher rolling resistance factor to sustain the same AoR as the very angular gravel fraction. However, since polyhedral non-round particles were used for the gravel, the rolling resistance is inherent in the particle shape, and the rolling resistance for these particles does not need to be included in the DEM model.

4.4 SURCHARGE ANGLES

Surcharge angles are not directly involved in transfer chute design, but are required to check the DEM model to make sure that the simulated cross-section on the discharge and receiving belts, and the bulk density of the simulated material on these belts are reasonable accurate. These results are generally used to adjust the solid fraction of the bulk material that is used to calculate the particle density.

Figure 4-15 shows that when the cylindrical pile formed by the mix of wet gravel and fines is agitated, the material falls into typical conical pile, showing that the bridging effect can be overcome if the un-compacted material is sufficiently disturbed. The Surcharge angle is not quite symmetrical, reflecting the different proportions of gravel and fines at various locations around the pile. The lumpiness caused by the gravel also resulted in some difficulties in accurately positioning the angle gauge.

Figure 4-15. Surcharge angle of wet -50 mm sample –left side.

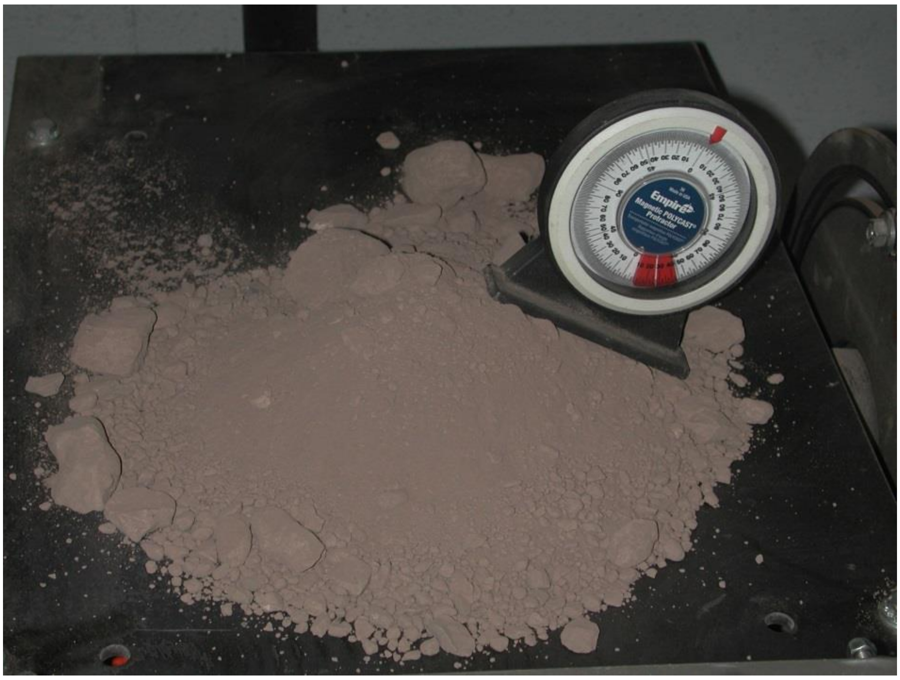

Figure 4-16. Surcharge angle of dry -50 mm sample – right side.

Figure 4- shows the surcharge angle of the dry -50 mm sample. The similarity in the surcharge angles of the dry -50 mm sample and the dry -6 mm fines indicates that the flowability of the mixed material is strongly influenced by the flowability of the fines fractions.

Figure 4-17. Surcharge angle of wet -6 mm fines – right side.

Figure 4-18. Surcharge angle of dry -6 mm fines – left side.

Figure 4-17 and Figure 4-18 show the surcharge angles for the wet and dry -6 mm fines.

Table 4- gives a summary of the surcharge angle results.

Material	Surcharge Angle Left	Surcharge Angle Right
	[deg]	[deg]
-50 mm sample - Wet	42	13
-50 mm sample -Dry	31	28
-50 mm to +6mm gravel - Dry	20	24
-6 mm fines – Wet	34	36
-6 mm fines - Dry	29	27

Table 4-4. Summary of surcharge angle results.

4.5 COMPRESSIBILITY

Most of the material properties are dependent on the consolidation stress, or impact pressure created by the force of impact. The magnitude of the impact pressure developed during the bulk material's impact on a chute or belt surface is dependent on the material's velocity and bulk density just prior to the impact. The consolidation stress generated during the UCS and CCS tests should encompass the range of potential impact pressures. The following calculation provides a fair estimate of the conditions required.

The impact pressure is generally expressed as

$$P = \gamma_B v_0^2 \sin^2\theta$$

Where

P = impact pressure, or normal consolidation stress, in Pa or N/m^2

γ_B = bulk density in kg/m^3

v_0 = impact velocity in m/s

θ = angle of impact

Since test forces are applied perpendicular to the boundary surface, only the normal (perpendicular to the target surface) component of this pressure is of concern. For the purposes of this calculation, only the material's vertical velocity component is used, and the angle of impact is taken to be equal to 90^o.

However, the bulk density factor in the impact pressure equation does not have a constant value when the bulk material is accelerating due to gravity during its vertical drop. The bulk density of a falling bulk material decreases as it disperses vertically due to the differential velocity created by the gravitational acceleration. There is also typically some horizontal dispersal, but for this analysis it is assumed that the horizontal cross-section of the material stream stays relatively constant.

The magnitude of the decrease (or increase) in bulk density of the falling material can then be determined for a given material drop height and mass flow rate. If a chute is fed by a conveyor carrying material at a given speed and a known bulk density, the change in bulk density caused by the vertical drop is proportional to the ratio of the conveyor speed and the impact velocity.

Figure 4-19 shows how the impact velocity and the normal stress on the material due to the impact vary as a function of the material drop height. Generally, a preliminary trajectory study is required to determine the maximum drop height for a given chute design. For the material under consideration, all internal baffles, rock boxes and ledges had been removed from the chutes on site due to plugging issues with the wet material, resulting in drop heights of approximately 7 m from the discharge pulley to the receiving belt. The typical normal stress due to the impact of the material on the receiving belt for this drop height, a mass flow rate of 1 500 tph, and a bulk density of 1 800 kg/m^3 is approximately 89 kPa.

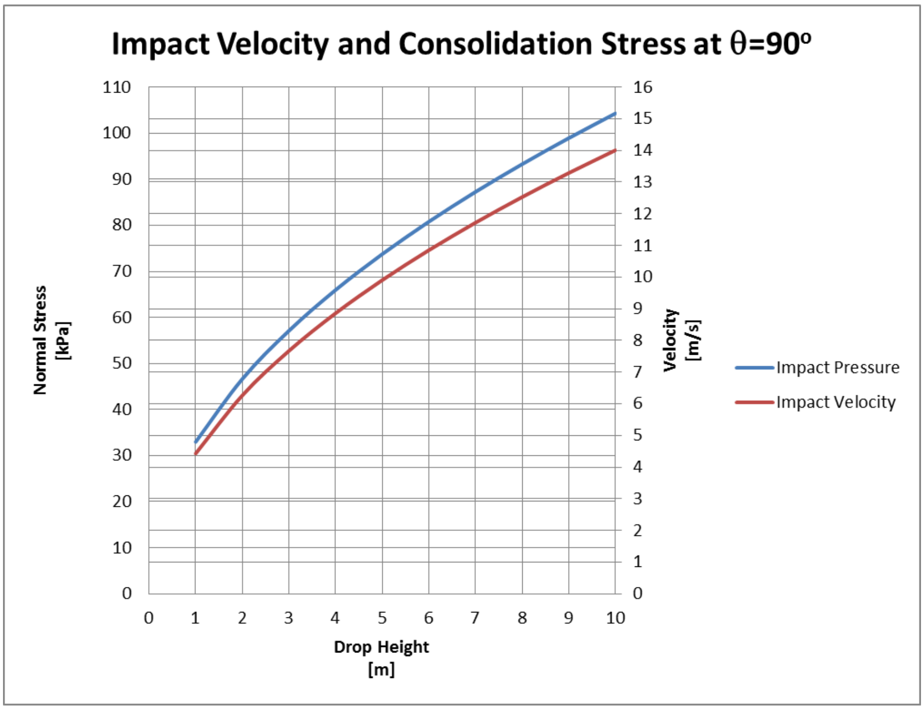

Figure 4-19. Impact velocity and normal consolidation stress.

As the material is compacted during the impact event, or by the weight of the material overburden, the particles are packed tighter together. For most bulk materials, when the solid fraction of the material exceeds more than about 0.65, the particles themselves will begin to deform, with the amount of deformation dependent on the material's strength and stiffness. Any moisture or air in the void spaces between the particles also tends to get squeezed out. This deformation increases the contact area between adjacent particles, which in turn increases the surface tension effects of any moisture in the void spaces, leading to adhesion at the impact surface and cohesion between the compacted particles.

The graphs in Figures 4-21 through 4-26 are used to determine the relative amount of compaction that occurs during an impact event, and establish limits on how much consolidation stress is acceptable for maintaining good material flow.

The UCS results are for unconfined material, typical of chute conditions, while the CCS results are for confined material, which is more typical of hopper or bin conditions. It can be seen that the UCS bulk densities of both the fines and gravel fractions approaches the measured value of the particle density (2 750 kg/m^3) as the consolidation stress increases.

This trend is strongest for the wet fines, and Figure 4-20 shows that at high consolidation stresses, the wet fines become a solid cake that adheres to the wall surface.

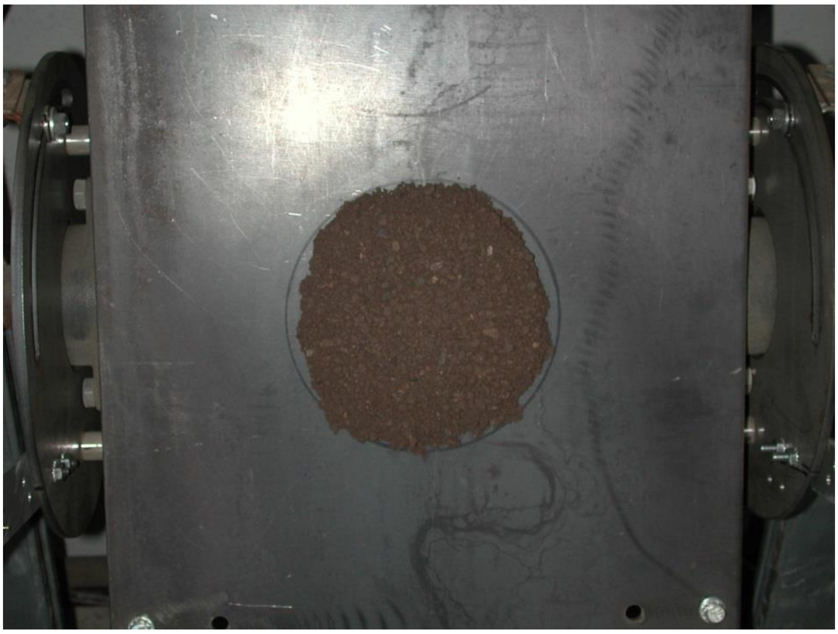

Figure 4-20. Compacted wet fines after UCS test (wall shown in vertical position).

In the CCS tests, the increase in bulk density is limited by the lack of horizontal degrees of freedom. The graphs show that as the consolidation pressure increases, the solid fraction of the material tends towards the theoretical close packing limit of approximately 0.65.

4.5.1 Wet fines (-6 mm)

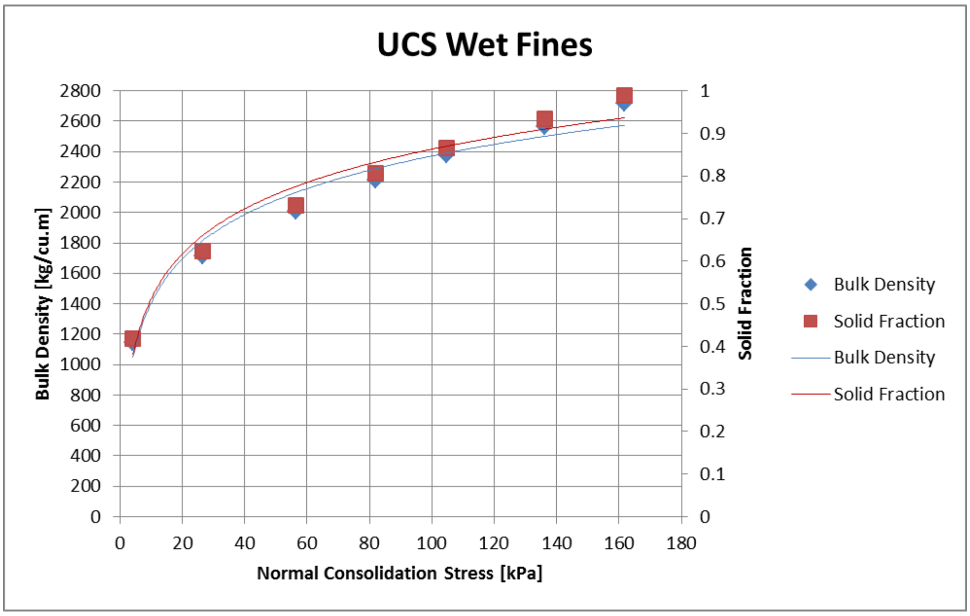

Figure 4-11. Unconfined compressibility ofwWet -6 mm fines.

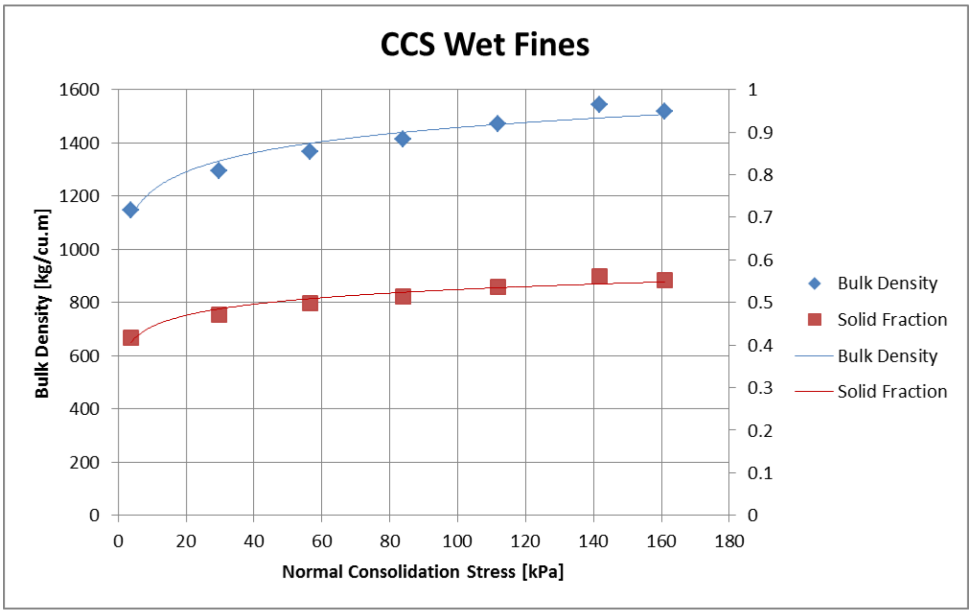

Figure 4-22. Confined compressibility of wet -6 mm fines.

4.5.2 Dry fines (-6 mm)

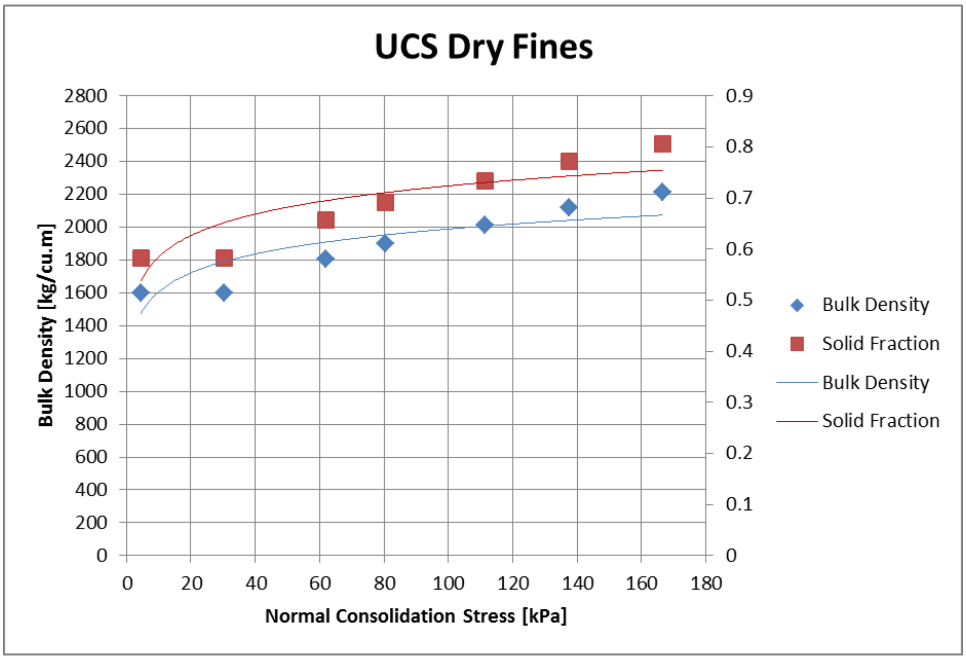

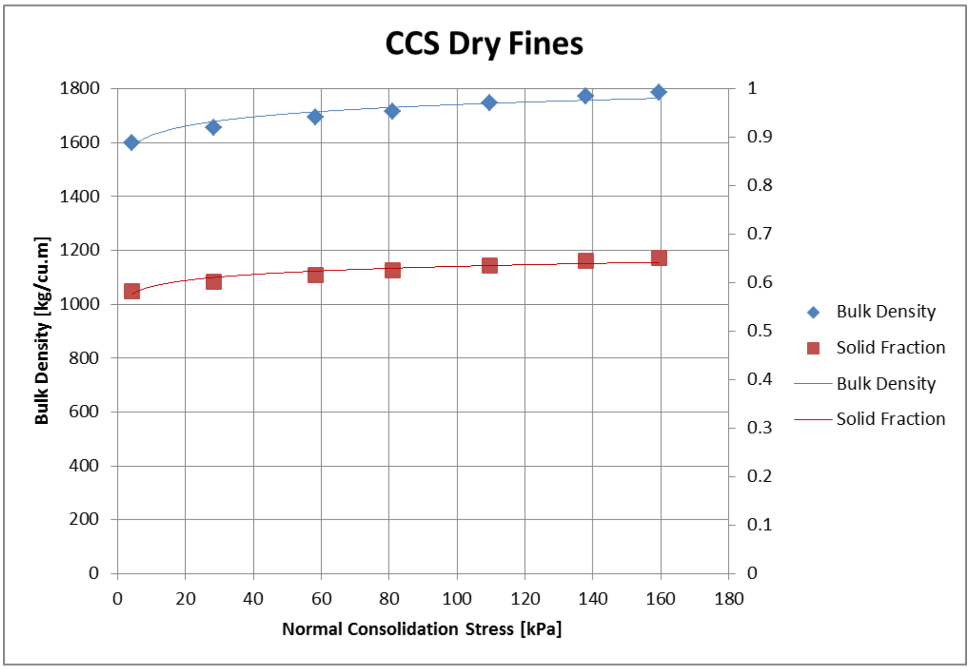

Figure 4-12. Unconfined compressibility of dry -6 mm fines.

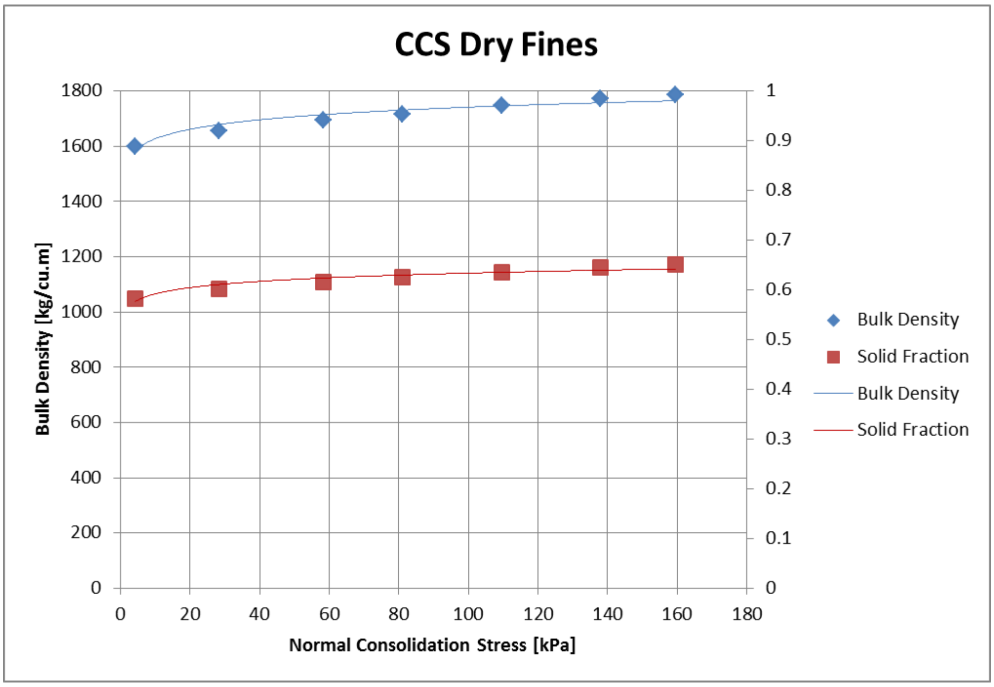

Figure 4-24. Confined compressibility of dry -6 mm fines.

4.5.3 Dry gravel (-50 mm to +6 mm)

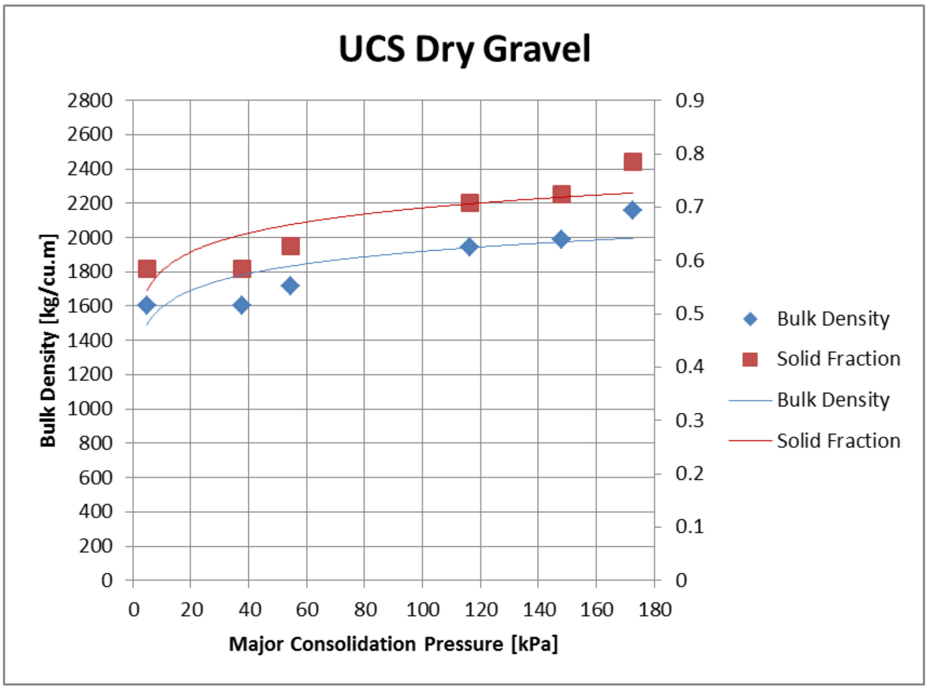

Figure 4-13. Confined compressibility of dry -50 mm to +6 mm gravel.

4.6 MATERIAL STIFFNESS

The bulk material stiffness's for all the particle fractions tend to increase linearly with the consolidation stress. The wet fines and dry fines results are more consistently linear, while the dry gravel fraction has some large deviations from the calculated best fit line. These outliers can be attributed to occasional large variations in the pressure plate displacement that occur when the larger gravel particles suddenly shift position or orientation as the load is applied to the test cell.

The UCS tests for the fines fractions give higher stiffness's for the same normal stress as the CCS test for the same particle fraction. This effect is more pronounced for the wet fines than for the dry fines. The dry gravel, allowing for the skew in the interpolation line due to the outliers, has very similar stiffness trends for both tests.

These test results show that the method achieves results for the material stiffness (Young's Modulus) that vary over the same order of magnitude (10^5 to 10^7 N/m^2) as those described in geotechnical data for compacted sand, clay and gravel materials found in typical undisturbed soil. These are interesting results which confirm the validity of the test procedure, but they are not very useful for DEM calibration, as the input parameter to be establish is the magnitude of the particle stiffness.

4.6.1 Wet fines (-6 mm)

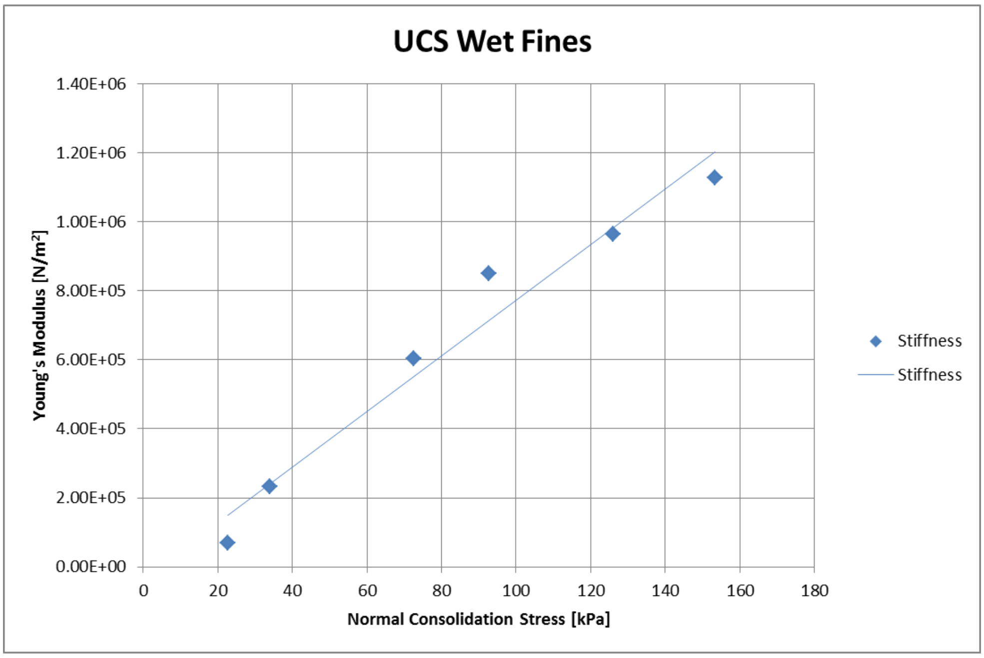

Figure 4-14. Unconfined material stiffness for wet -6 mm fines.

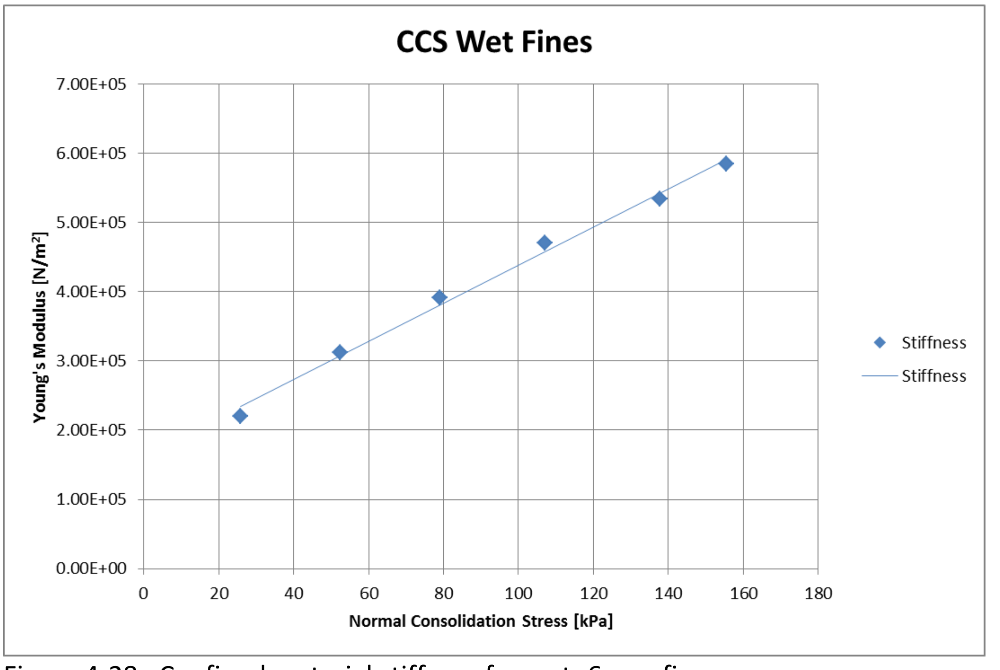

Figure 4-28. Confined material stiffness for wet -6 mm fines.

4.6.2 Dry fines (-6 mm)

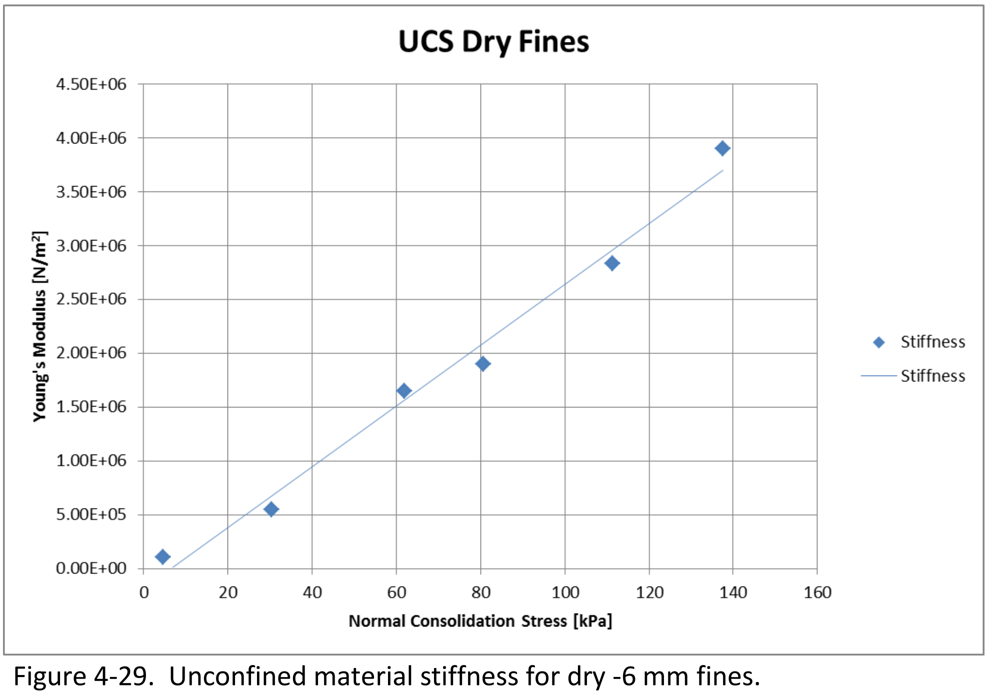

Figure 4-29. Unconfined material stiffness for dry -6 mm fines.

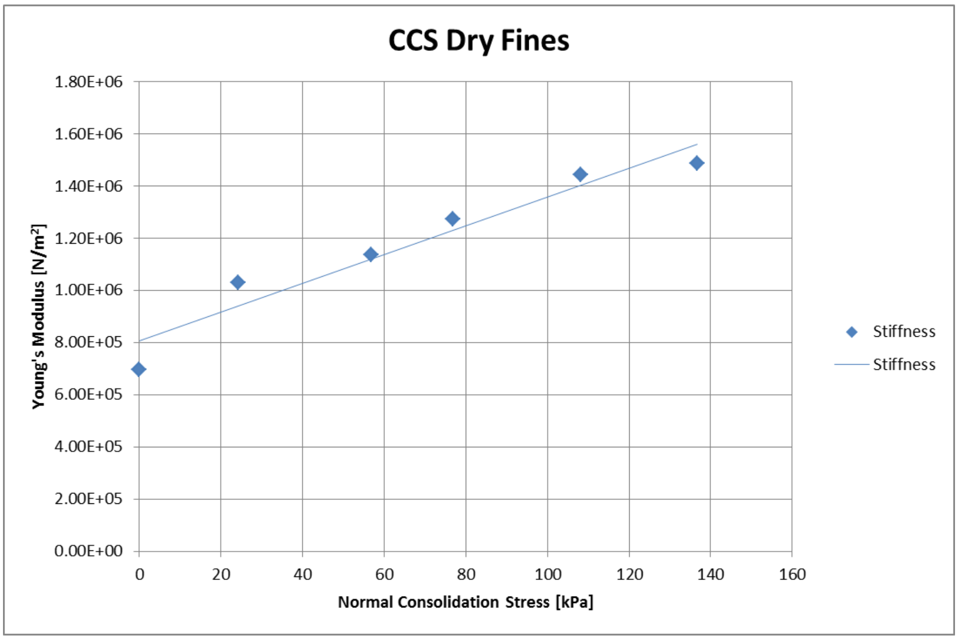

Figure 4-30. Confined material stiffness for dry -6 mm fines.

4.6.3 Dry gravel (-50 mm to +6 mm)

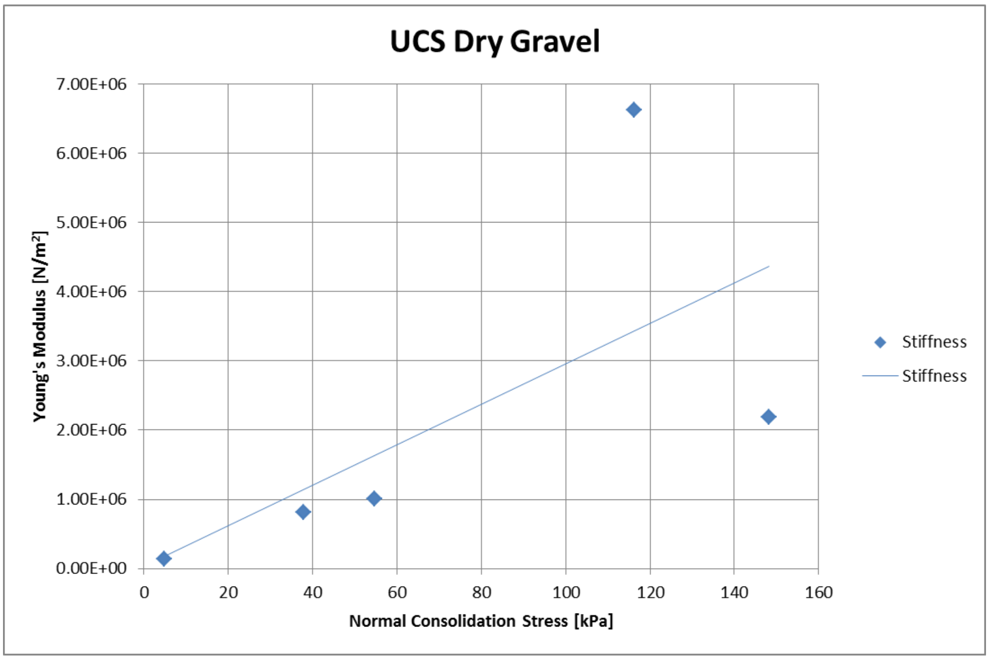

Figure 4-31. Unconfined material stiffness for dry -50 mm to +6 mm gravel.

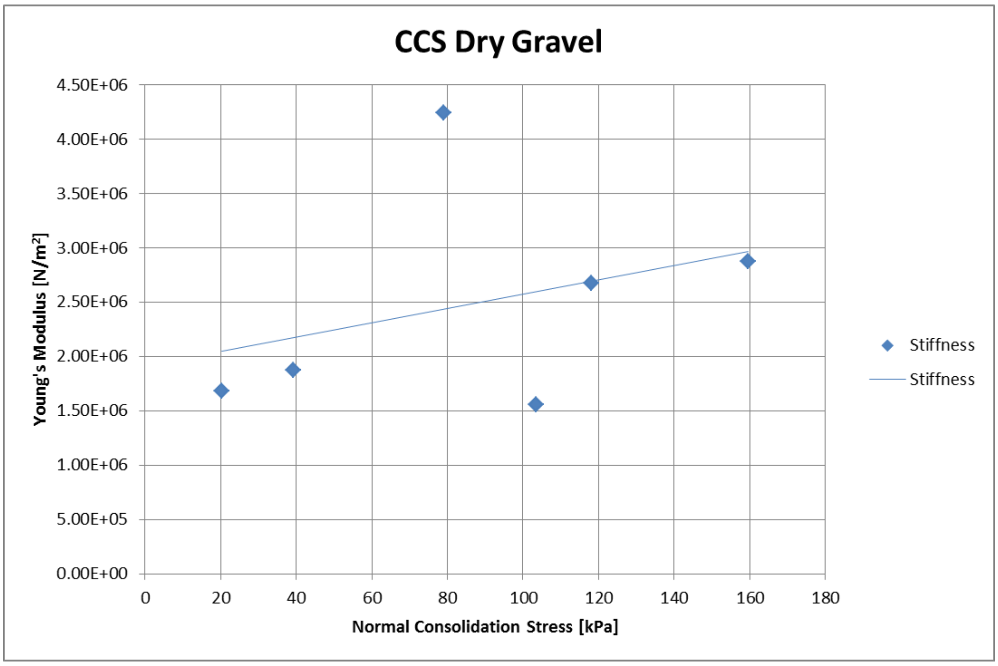

Figure 4-32. Confined material stiffness for dry -50 mm to +6 mm gravel.

4.7 PARTICLE STIFFNESS

To get a good estimate of the particle stiffness, the CCS expansion test was developed. The initial high consolidation stress assures better particle-to-particle contact, and results in a more consistent value for the Young's modulus over the range of consolidation pressures tested. The wet fines were not tested, as the need for the CCS expansion test was not realised until after the material had been thoroughly dried.

The graphs in Figure 4-33 and

Figure 4-34 show that the dry fines and the dry gravels gave very similar results during the CCS expansion test, and provide a particle stiffness that remains fairly constant over a wide range of normal consolidation stresses. The drop off at low stress can be attributed to the loss of contact between particles as the bulk material expands.

Here it is seen that the particle stiffness for both the dry fines and the dry gravel is approximately 6×10^6 N/m^2.

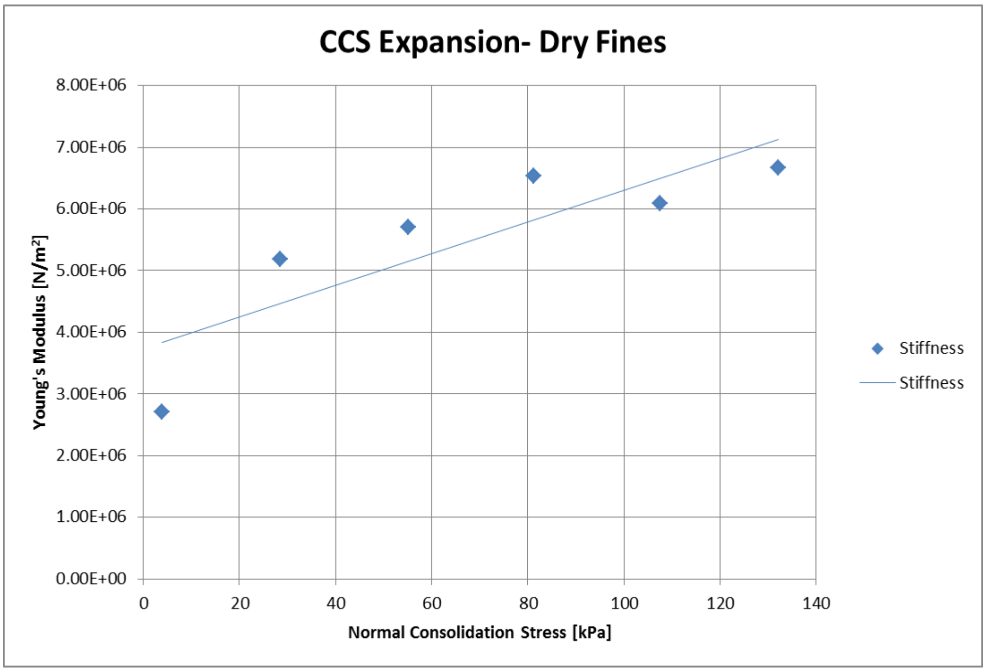

Figure 4-33. Particle stiffness for -6 mm dry fines.

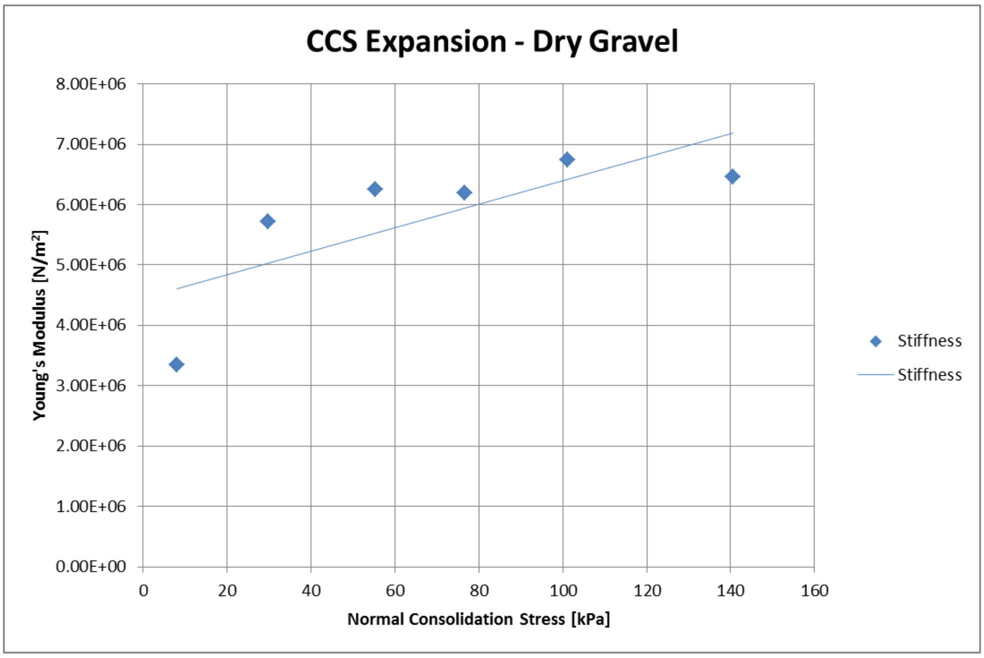

Figure 4-34. Particle stiffness for -50 mm to +6 mm dry gravel.

4.8 WALL FRICTION COEFFICIENTS

Comparison of the wet fines friction coefficients and the dry fines at the same magnitude of normal consolidation stress shows how big an effect even 5% of moisture in the fines can have on these coefficients.

The wall friction coefficients for the dry fines approach constant values of about 0.5 (static friction) and 0.6 (dynamic friction) for consolidation stresses above 60 kPa. Similarly, the dry gravel wall friction coefficients approach a constant value of about 0.5 (both static and dynamic friction) for consolidation stresses above 30 kPa. This result is probably due to the material reaching its limit of compressibility due to high stiffness of the particles.

On the other hand, the wet fines show no such plateau, due to the additional adhesive forces between the particles and the boundary plate created by the moisture content. Note that the intercepts of the static and dynamic coefficient lines for the wet fines are approximately equal to the constant values determined for the dry fines.

4.8.1 Wet fines (-6 mm)

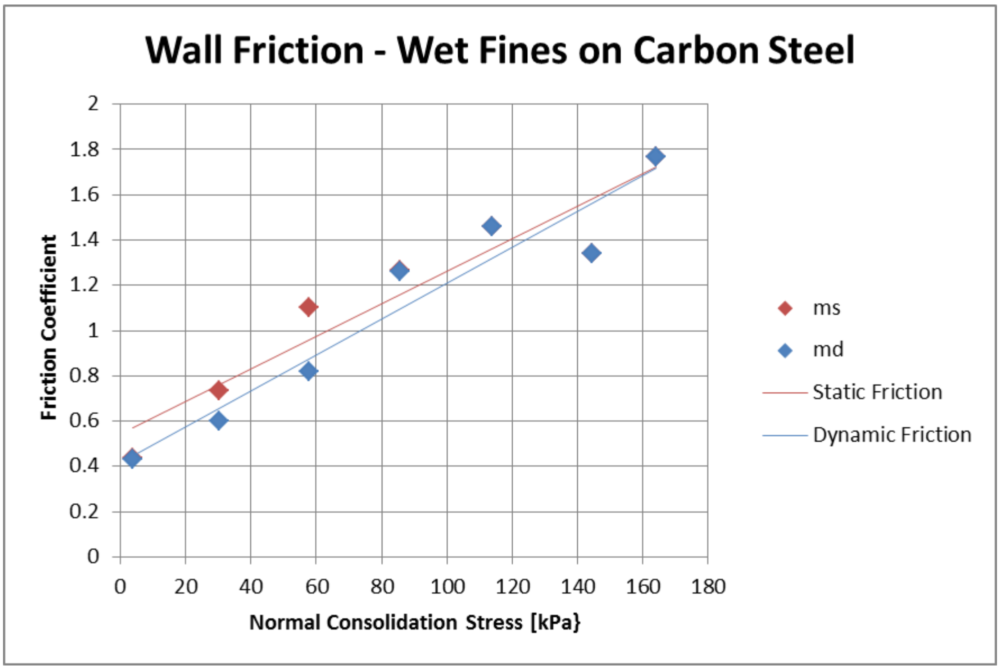

Figure 4-35. Wall friction coefficients for wet fines (ms = μ_s, md = μ_d).

4.8.2 Dry fines (-6 mm)

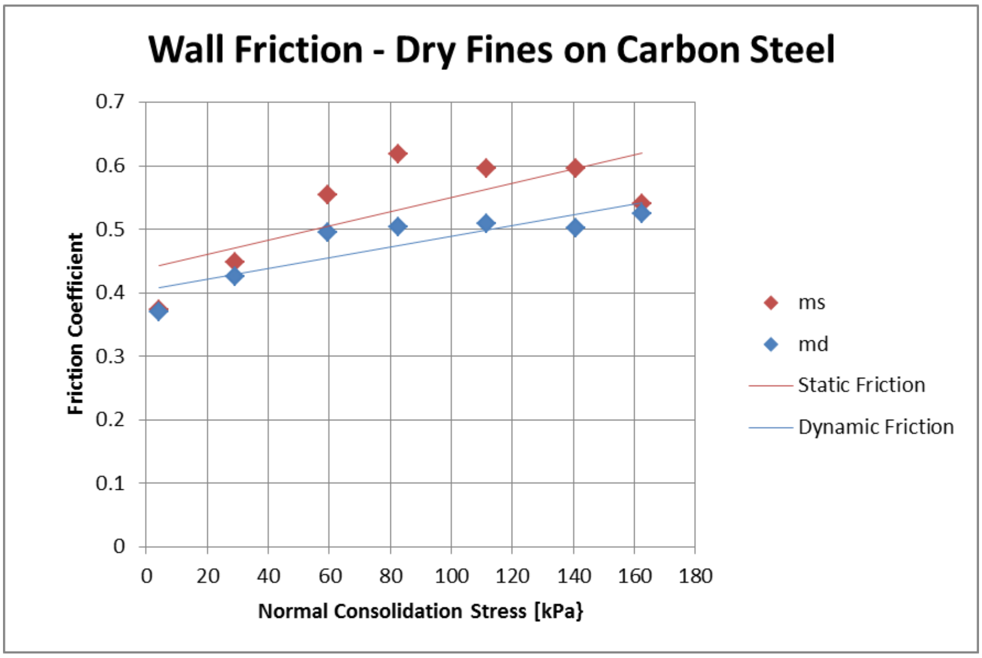

Figure 4-36. Wall friction coefficients for dry fines (ms = μ_s, md = μ_d).

4.8.3 Dry gravel (-50 mm to +6 mm)

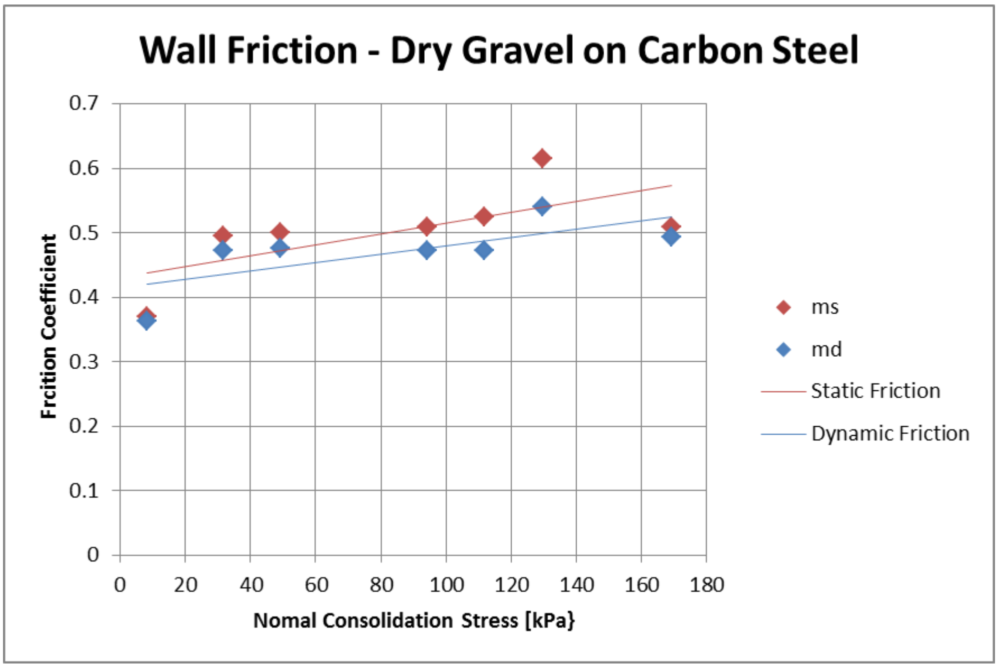

Figure 4-37. Wall friction coefficients for dry gravel (ms = μ_s, md = μ_d).

4.9 INTERNAL FRICTION COEFFICIENTS

Internal friction coefficients for the wet fines were difficult to obtain for consolidation pressures above 55 kPa. At the higher consolidation pressures, the test cell moved more than 1 mm (the precision limit of the motion sensor), but less than 10 mm, regardless of the slope of the shear plane with respect to gravity. Even at lower consolidation pressures the elapsed time of the test cell motion was so large that the static and dynamic friction coefficients were effectively equal.

Figure 4-38 shows the mobile test cell suspended by the cohesion between the material in the mobile half and the material in the stationary half, at a consolidation stress of 86 kPa and a tilt angle of 90 degrees. Based on the consolidation stress curve shown in Figure 4-13, this would represent a chute drop height of about 6.5 metres, but this level of cohesion could be occurring when the consolidation pressure is as low as 60 kPa, at a drop height of 3.5 m.

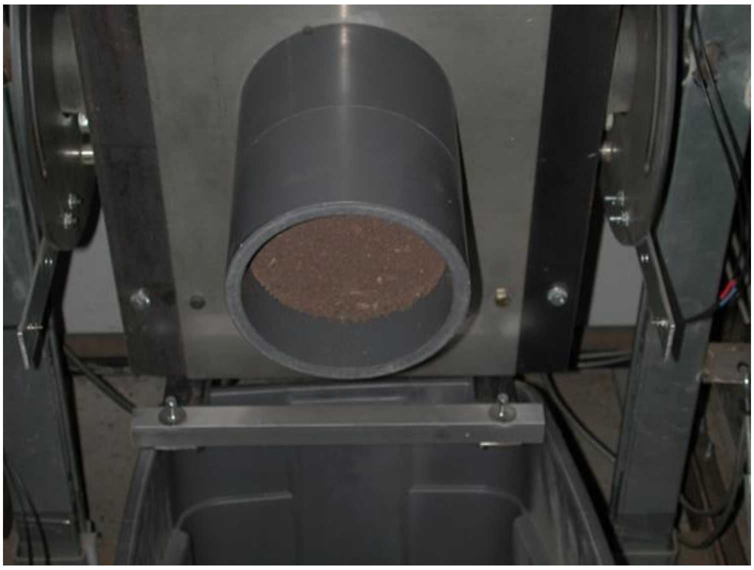

Figure 4-38. Cohesion between wet fines at 86 kPa (wall shown in vertical position).

The wet fines and dry fines both show a linear increase in friction as the consolidation pressure increases. This implies that there are active cohesive forces in both samples, although much less in the dry fines than in the wet fines. Note that the intercept for the wet fines is approximately equal to the intercept for the dry fines at around 0.4 to 0.6. These values are very close to the previously determined intercepts for the wall friction coefficients.

The almost flat slope shown in Figure 4-41 shows that there are almost no cohesive forces between the gravel particles, and that the internal friction coefficient for a bulk sample of these particles is approximately 0.8.

4.9.1 Wet fines (-6 mm)

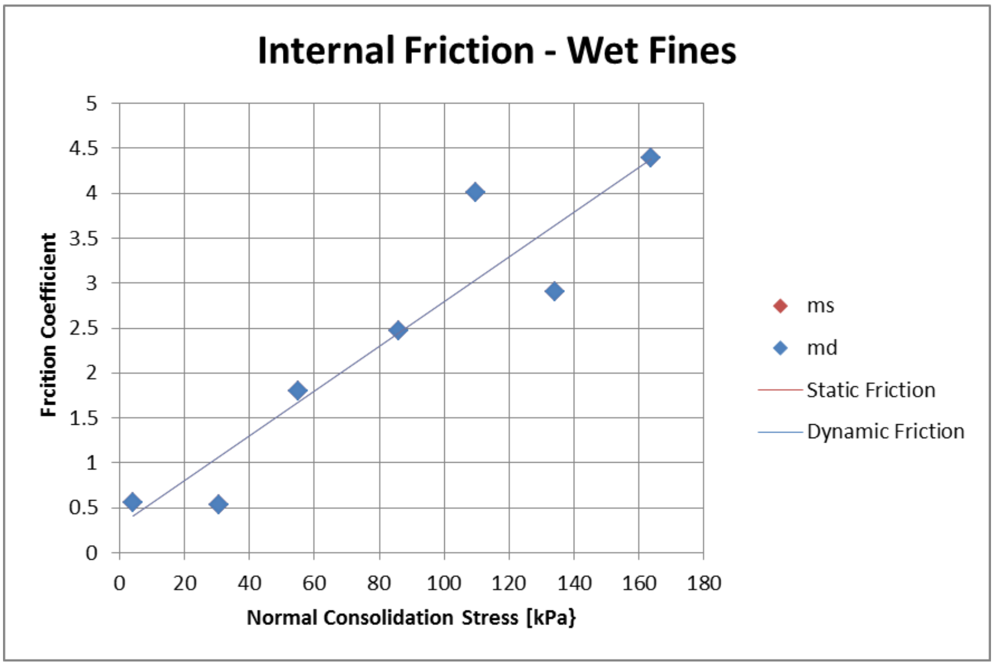

Figure 4-39. Internal friction coefficients for wet fines (ms = μ_s, md = μ_d).

4.9.2 Dry fines (-6 mm)

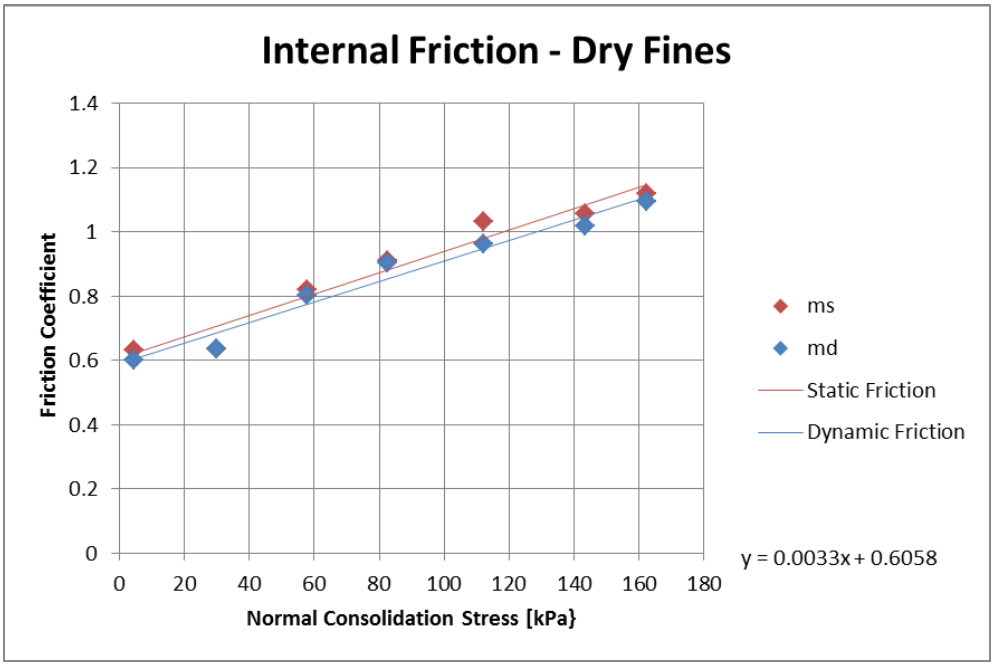

Figure 4-40. Internal friction coefficients for dry fines (ms = μ_s, md = μ_d).

4.9.3 Dry gravel (-50 mm to +6 mm)

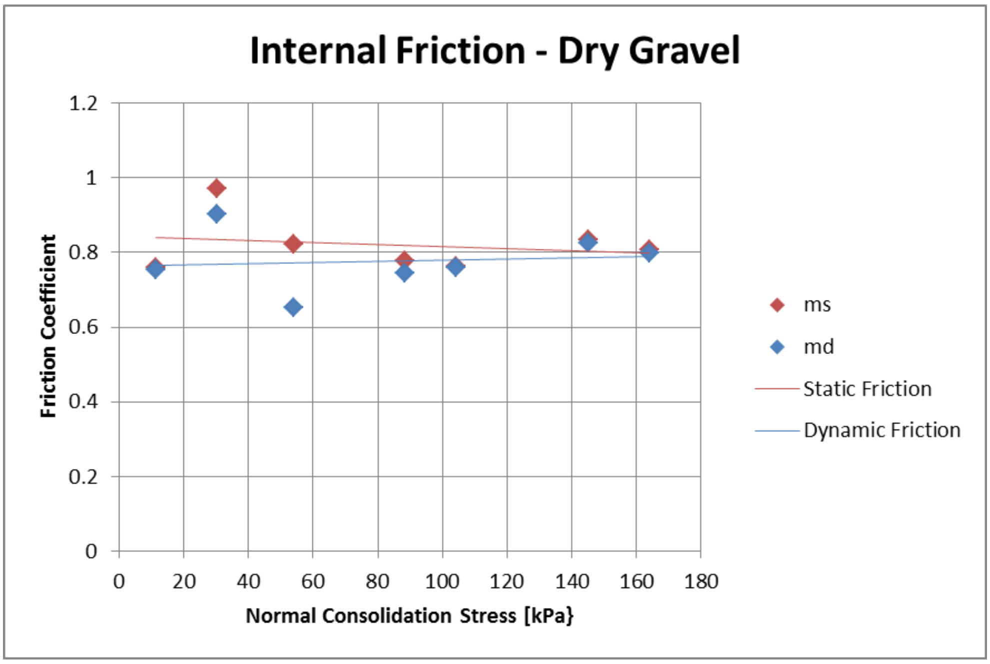

Figure 4-41. Internal friction coefficients for dry gravel (ms = μ_s, md = μ_d).

5. DEM CALIBRATION MODEL

It is important to note that the DEM calibration parameters given here are specifically determined for ROCKY DEM software, and may or may not be compatible with other DEM software. It is also important to note that additional DEM studies and comparisons with existing chutes transferring this material are required to verify that the simulated material behaves similarly to the real material. This is particularly true for any simulation involving wet material.

The DEM calibration serves as a bridge between the real material properties, with the complete range of particle sizes, and the DEM model, which has computational limits on the size of the smallest particle that can be represented and still get a design flow solution in a reasonable amount of computer run-time. In this case, as for most transfer chute designs, the smallest particle included in the DEM model is 25 mm in diameter.

The computational algorithm uses a simplified model of how the particles behave during these interactions. For example, real particles can undergo permanent deformations, up to and including fracturing into smaller particles. In the ROCKY DEM algorithms used for chute design, instead of deforming or fracturing during impact, the particles maintain their shape and integrity, but are allowed to overlap each other in a way that approximates the degree of deformation expected due to the particle stiffness.

For the relatively few large particles that are larger than 25 mm, the properties measured in the material tests can be used directly. However, for the -25 mm fractions, the material properties must be adjusted so that the various classes of 25mm particles mimic the behavior of the actual fines and gravels that those particles represent. In particular, adjustment of the particle stiffness may be needed, and to a lesser extent the various frictions factors, in order to make the 25 mm DEM particles behave like the -25 mm particles they represent.

Many of the calibration parameters will be highly dependent on the normal consolidation pressure, which itself is dependent on the actual chute geometry, including belt speed, drop height and material trajectory. An initial trajectory analysis of a proposed chute design is generally required to estimate the maximum consolidation stress the particles will experience during their transit through the chute. Once the maximum normal consolidation stress that will occur in the chute is known, the material calibration can be refined to match the chute geometry requirements. However, this stage of the calibration is not included in the present scope of work.

Calibration parameters for the -6 mm wet fines are dependent on the actual moisture content, and are only suitable for simulations of this material with a 5% moisture content. Additional testing would be required to determine the correct parameters for alternate moisture content levels.

5.1 LIMITATIONS OF DEM TEST MODELS

The key to this calibration procedure is the accurate modelling of the various control surfaces; the steel plate that applies pressure to the sample in the test cell; the cylindrical test cell itself; and the bearing plate that the sample slides on in the wall friction tests. There are some limitations to the ROCKY DEM program that limited the accuracy and precision of the DEM models.

1. Tilting the bearing plate. This was not possible, as boundary surfaces, such as the test cell, are not affected by the gravitational forces that get applied to the particles. The motions of the test cell had to be programmed into the simulation. Instead of tilting the bearing plate and allowing the simulated gravitational force to apply tangential forces along the tilted plate, it was necessary to program a sequential series of increasing tangential forces directly to the test cell. The tangential forces were applied in 5 N increments. Since the simulated mass of the material and the test cell was approximately 26 N, the precision in the friction coefficients derived from the simulations is on the order of ±0.2.

2. Number of particles in the simulated test cell. The number of un-compacted 25 mm DEM particles that would fit in the simulated test cell, which was exactly the same size as the real test cell, was approximately 100. Of these only about 25 were in actual contact with the bearing plate surface. This is at the lower limit for a statistical sample, and some variation in the DEM results due to statistical variations occurred.

3. Depth of the shear plane in the internal friction simulations. Due to the 25 mm DEM particle size, in order for shearing action to take place, significant vertical motion of the mobile test cell had to occur to allow the particles to slip past each other. No doubt similar particle motion occurred during the actual test, but the depth of the shear plane for -6 mm particles is of the order of 3 mm, and would be difficult to observe during the test. The equivalent vertical displacement in the DEM simulations could be as much as 12 mm.

5.2 PARTICLE SIZE DISTRIBUTION AND PARTICLE SHAPES

The DEM particle size and shape distribution includes the following classes of particles:

DEM Particle Classes							
Class	**DEM Particle Size**	**% Passing**	**% Oblong**	**% Rounded**	**% Slab**	**% Spheres**	**Material Type**
Boulders	-200 mm	100	0	100	0	0	M1
Large cobbles	-150 mm	95.1	20	50	30	0	M1
Medium cobbles	-100 mm	85.0	20	50	30	0	M1
Small cobbles	-75 mm	77.0	20	50	30	0	M1
Large gravel	-50 mm	73.6	20	50	30	0	M1
-25 mm to +6 mm gravel	25 mm	70.0	0	0	0	100	M2
-6 mm fines	25 mm	37.4	0	0	0	100	M3

Table 5-1. DEM particle classes.

The smallest particles included in the DEM simulations were 25 mm diameter spheres. Except for the 25 mm particles, all the other particles are represented in the same proportions as determined by the photographic analysis of the in situ material. The +25 mm to -50 mm fraction was used to correlate between the size analysis done using photographic analysis and that performed by subsequent sieve analysis of the -50 mm sample shipped to the lab.

5.2.1 Particle Shapes

Particle shapes and the relative percentage of each shape in each size class were determined by visual inspection of photos taken on site and photos taken during the calibration tests.

Name	Shape	Vert. Aspect Ratio	Horz. Aspect ratio	Smoothness	No. of Corners	Superquadric Degree
Oblong		1.7	0.7	0.1	5	2.0
Rounded		1.0	1.0	0.2	6	7.0
Slab		0.5	1.0	-	10	8
Sphere		-	-	-	-	-

Table 5-2. Particle shape factors.

NOTE: Aspect ratios are per ROCKY DEM input requirements. It should be readily apparent that a simple 90 degree rotation of a slab with a vertical aspect ratio of 0.5 turns it into a slab with an aspect ratio of 2.0.

5.2.2 Material Types

Due to the differences between the dry fines and wet fines, two separate, complete particle sets are required. For DEM simulations of dry conditions, the M3 material properties are derived from the -6 mm dry fines test results. For DEM simulations of wet conditions, the M3 material properties are derived from the -6 mm wet fines test results.

Thus, there are three basic material types required for each particle set:

- M1 – Material properties derived from -50 mm to -6 mm gravel test results
- M2 – Material properties derived from -50 mm to -6 mm gravel test results, but with adjustments to the material stiffness and rolling resistance factors included
- M3 – Material properties derived from -6 mm fines test results.

NOTE: Any cohesive force factors only apply to particle-to-particle interactions for the wet fines and dry fines fraction. The particle-to-particle interaction between the wet fines and the gravel fractions should use the same adhesive force factor used between the fines and the boundary surfaces.

5.3 BOUNDARY SURFACE DENSITY AND STIFFNESS

DEM program instructions frequently tell users to use a relatively high default value of 10^{11} N/m^2 for boundary surface stiffness's. In the interest of more realistic interactions between the particles and the boundary surfaces, actual known values were used for the materials in the test apparatus boundaries. The user should be aware that low values of both boundary and particle stiffness's can result in the particles passing through the boundary when the action of high normal forces results in the contact overlap distance exceeding the particle radius.

Boundary Surface	Boundary Material	Density [kg/m^3]	Stiffness (Young's Modulus) [N/m^2]
Pressure plate	Carbon steel	7850	2.38x10^{11}
Bearing/sliding plate	Carbon steel	7850	2.38x10^{11}
Test cell	PVC pipe	1400	2.55x10^{9}

Table 5-3. Boundary materiapProperties.

Table 5-3 shows that the default stiffness is of the same order of magnitude as steel, and only about 50 times the stiffness of PVC.

5.4 ROLLING RESISTANCE FACTORS

Rolling resistance factors are independent of the normal consolidation stress for dry materials with no adhesive or cohesive properties. However, the particle shapes have a big influence on the particle rolling resistance, as spherical and rounded particles roll more easily than oblongs and slabs.

The shape analysis performed on the in situ bulk material and on the particles using photographic and microscopic observations indicates that the particle shapes are relatively scale insensitive. That is, the small fines particles have roughly the same shapes and the same shape distribution as the larger gravel particles.

For the large gravel particles, which can be modelled in ROCKY DEM as non-round particles, the rolling resistance will be determined by the particle shapes and their interactions within the DEM model. The rolling resistance factor for these particles should be set to 0.0.

For the small gravel particles, and the fines particles, both of which are modelled as spherical particles to improve the computational speed, rolling resistance factors must be input to account for the observed non-round shapes. To determine the magnitude of this factor, a DEM study published in 2012, by Wensrich and Katterfeld[1] is consulted. Figure 5-1 shows Figure 6 of this paper, which gives an estimate of the rolling friction based on the observed aspect ratio of the particles.

Based on the particle shapes observed, about 50% of the particles are oblongs and slabs with aspect ratios in the range of 1.7 to 2.0. The remaining rounded particles have an aspect ratio of 1.0. Taken as a whole, the average aspect ratio is estimated to be around 1.7, giving a coefficient of rolling friction (rolling resistance factor) of about 0.35.

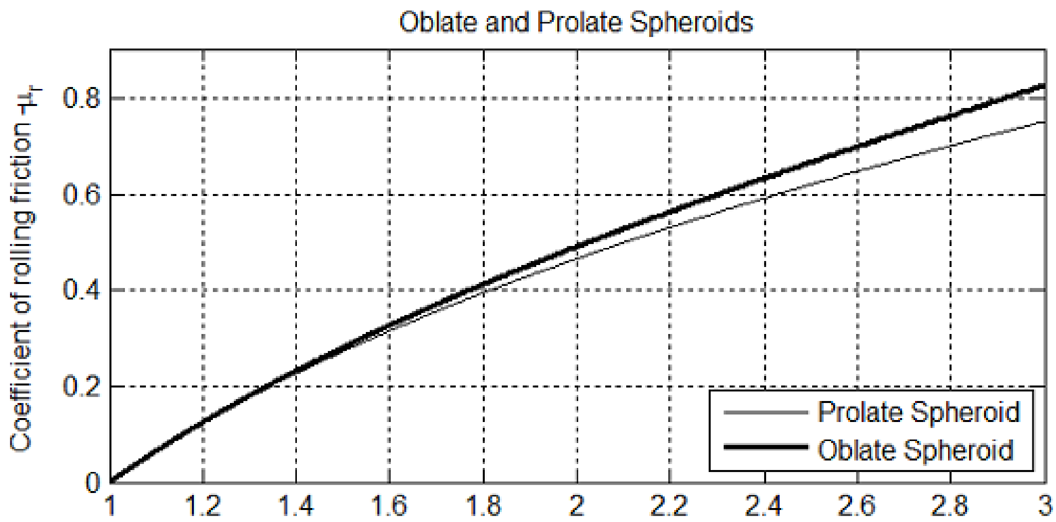

Aspect ratio – major / minor axis

Figure 5-1. Calculated values of the estimated coefficient of rolling friction.

Wensrich and Katterfeld (2012)

As a further check on this estimate, Wensrich and Katterfeld have provided results of angle of repose (AoR) simulations that correlate the particles internal friction coefficient (μ_p) with the rolling friction coefficient (μ_r). The resulting graph, which is Figure 9(b) in their paper, gives contours for the AoR achieved for the combination of these coefficients for a set of spherical particles. This graph is shown in Figure 5-2 below.

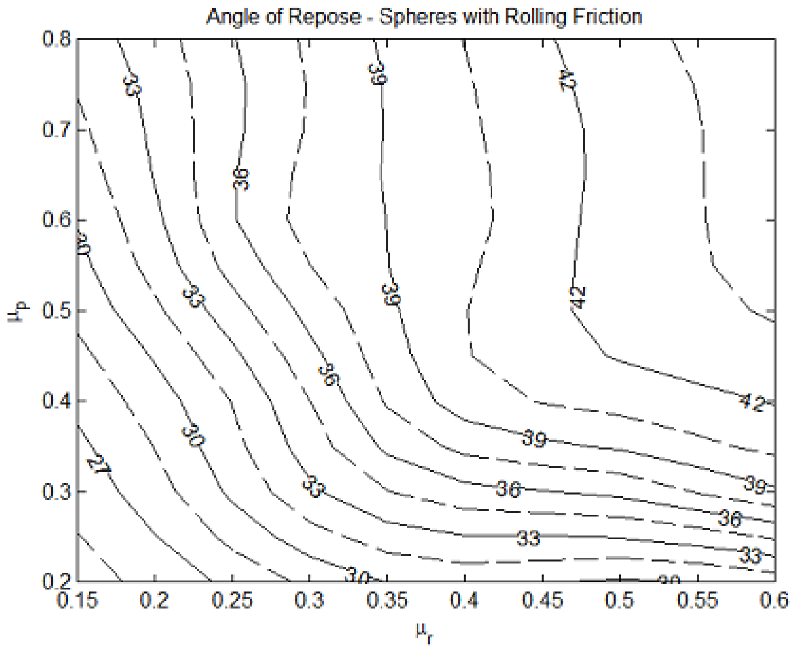

Figure 5-2. Angle of repose for spheres with rolling friction.
Wensrich and Katterfeld (2012)

Based on the observed AoR of the +6 mm to -50 mm gravel and the -6 mm fines (wet and dry), and internal friction coefficients of 0.5 to 0.8, Figure 5-2 shows that 0.35 is the minimum rolling resistance factor that should be used for 25 mm spherical particles.

A DEM calibration model that replicates the conditions of the AoR test is used to determine the angle of repose for the spherical gravel and fines particles, and the rolling resistance factors are adjusted upward from the initial estimates until the angles of repose in the DEM models closely match the angle of repose observed in the laboratory tests. For these models, the following input parameters were used:

- Particle densities based on the bulk densities of the un-compacted material. The AoR test is performed on un-compacted material.
- Static and dynamic coefficients from the lowest consolidation pressure measured in the wall and internal friction tests. Again, the AoR test is done on un-compacted material, with very low normal consolidation stresses.
- Material stiffness equal to the stiffness of the dry fines and dry gravel derived from the CCS expansion tests and subsequent DEM simulations of the CCS friction tests.

It is assumed that any difference between the AoR for the dry fines and the wet fines would be due to cohesion.

Once the cohesive and adhesive force factors have been determined, the wet fines fraction in the DEM particle set are run through the AoR simulation to confirm conformance to the test results.

5.4.1 DEM AoR Results

Table 5-4 provides a comparison between the actual test results and the DEM simulations. Due to the coarseness of the particle set, the DEM angles of repose are difficult to measure accurately, but the simulations are a good qualitative fit to the test results. Another side effect of the coarseness of the particle set is that the AoR for the wet fines more closely resembles the results from the -50 mm wet sample than it does the -6 mm wet fines. At present, simulations on mixed particle sets are still in process, and no DEM results are available for comparison to the AoR test for the -50 mm wet sample.

Material Description	Material Type	Test		DEM	
		AoR Left [deg]	AoR Right [deg]	AoR Left [deg]	AoR Right [deg]
-25 mm to +6 mm - Dry gravel	M2	39	45	40	44
-6 mm fines - Dry	M3 – Dry	38	38	39	41
-6 mm fines - Wet	M3 - Wet	38	42	39/90	90
-50 mm sample - Wet	Mixed	90	90	-	-

Table 5-4. Comparison of AoR tests and AoR from DEM.

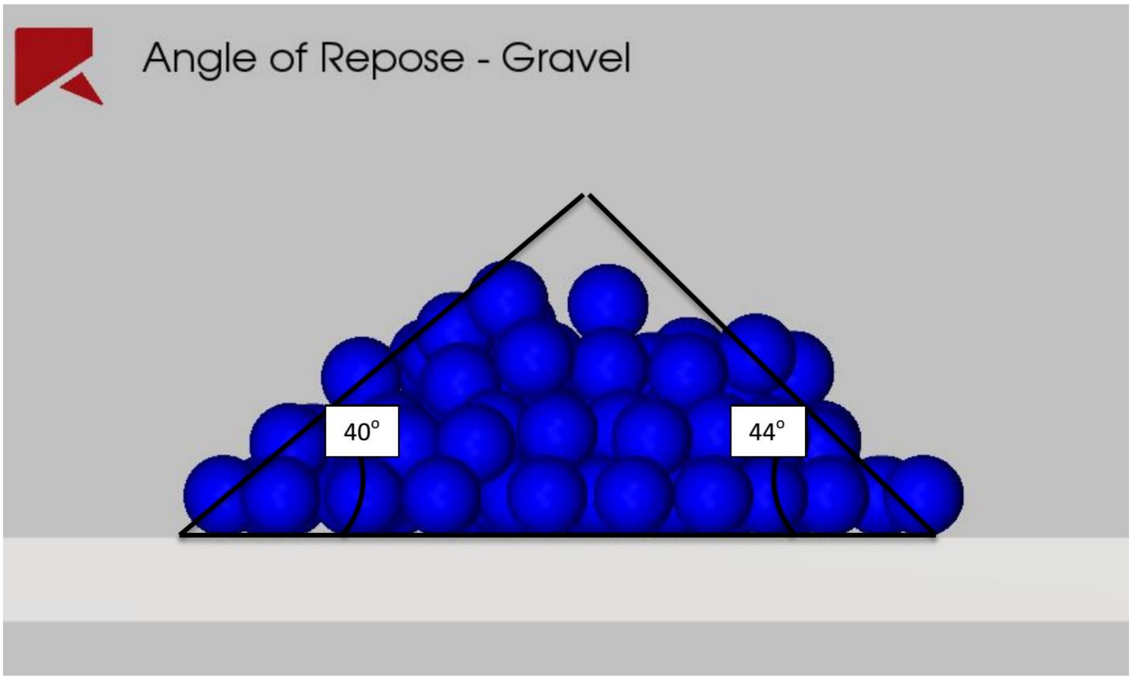

Figure 5-3. DEM AoR – dry gravel.

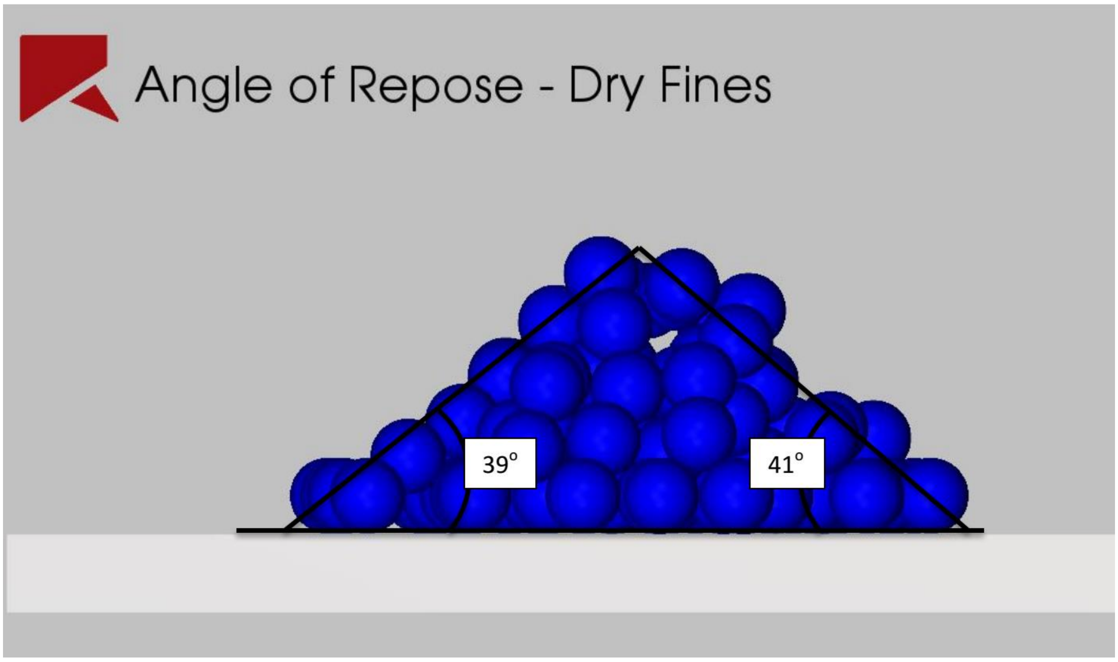

Figure5-4. DEM AoR – dry fines.

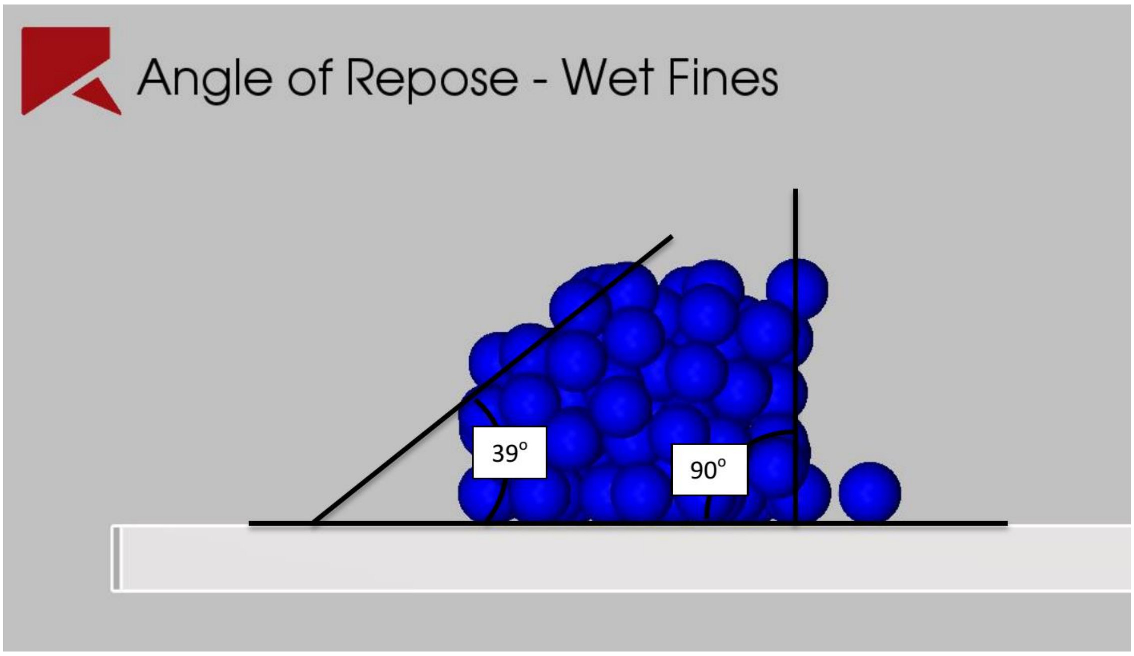

Figure 5-5. DEM AoR – wet fines.

Table 5-3 shows the rolling resistance factors at the end of the simulation iterations, which indicate that the initial estimates based on Wensrich and Katterfeld are consistent with the particle behavior observed in these tests and simulations.

Material Type	Rolling Resistance Factor
M1	0.00
M2	0.35
M3 – Dry	0.35
M3 - Wet	0.35

Table 5-3. DEM rolling resistance factors.

5.5 PARTICLE DENSITIES

While the larger, non-spherical particles can be adequately modelled using the particle density for the gravel found in the material tests, the 25 mm DEM particles must have their particle densities adjusted so that a full test cell in the DEM simulation has the same mass of particles as a full test cell in the actual tests.

To accomplish this, one must run iterations on a simulated test cell fill as part of the friction test simulation sequence, and adjust the particle density until the mass of the DEM particles equals the mass of the test material, as calculated based on the bulk density of the material type being simulated and the volume of the test cell. In order to do this properly in ROCKY DEM, it is necessary to NOT check the bulk density in the material specification window and set the solid fraction input to 1.0. This is necessary, as otherwise ROCKY DEM calculates the particle density based on the bulk density and the solid fraction. Other DEM programs may require different adjustments to achieve the same result.

This only really becomes a problem when all of the material types are eventually combined into a single particle set, as ROCKY DEM only allows one solid fraction input for an entire particle set in any given simulation.

Table 5-4 gives the particle densities required to achieve the un-compacted bulk densities measured in the tests for each material type.

Material Type	Particle Density [kg/m^3]
M1	2750
M2	3274
M3 – Dry	3337
M3 - Wet	2482

Table 5-4. DEM particle densities.

5.6 PARTICLE STIFFNESS AND FRICTION COEFFICIENTS

Particle stiffness's for the -200 mm to +25 mm gravel particles are taken from the CCS expansion test results with no modifications necessary.

For the -25 mm to +6 mm gravel fraction and the -6 mm fines fractions (wet and dry), the particle stiffness's must be modified to account for the differences between the single particles in the DEM model and an equivalent quantity of the bulk material represented by the 25 mm DEM particles.

The required adjustment in the particle stiffness's is determined using a DEM calibration model that replicates the conditions of the wall and internal friction tests. The particle stiffness's for the various 25 mm DEM particle types are adjusted until the simulation results closely approximate the actual test results. A pair of force vs displacement curves developed from the wall and internal friction test results are used to determine the required particle stiffness for the M2 and M3 material types.

Starting with the 6.0×10^6 N/m^2 stiffness estimate from Section 4.7, and wall and internal friction coefficients found for the dry gravel and the dry fines in Section 4.8 and 4.9, the DEM model of each friction test undergoes a series of iterations while varying the stiffness's and friction factors until the following factors have been optimized:

1. Stiffness and friction coefficients for a given material type are the same for both the wall friction and the internal friction simulations
2. Wall and internal friction curves are both good matches to the test data
3. Spring curves for the wall friction and internal friction tests are relatively close to the spring curves derived from each test.

This process requires multiple iterations of four different simulations at seven to eight different consolidation pressures. Thanks to the relatively small particle count involved, each combination of stiffness, friction coefficients, and consolidation pressure can be simulated using a relatively low-powered (8 CPU) desktop computer in less than five minutes. If a GPU processor is available, the solution time per combination can be significantly reduced.

5.6.1 Dry gravel

Figure 5-6 shows the final spring curve and friction curve for the dry gravel (M2 material) for the wall friction test. The accompanying table gives the particle stiffness and friction factors required to make this match. Note that the DEM particle friction coefficients are significantly different from the bulk material friction coefficients measured in our tests.

An internal friction test was not performed on the gravel fraction, as the interlocking of the large particles prevented any motion of the test cell. Based on the graph in Figure 5-2, the internal friction coefficients were expected to be higher than the value given here, and the need for additional iterations is indicated to bring the various friction factors into closer alignment with both the test results and with Wensrich and Katterfeld’s work.

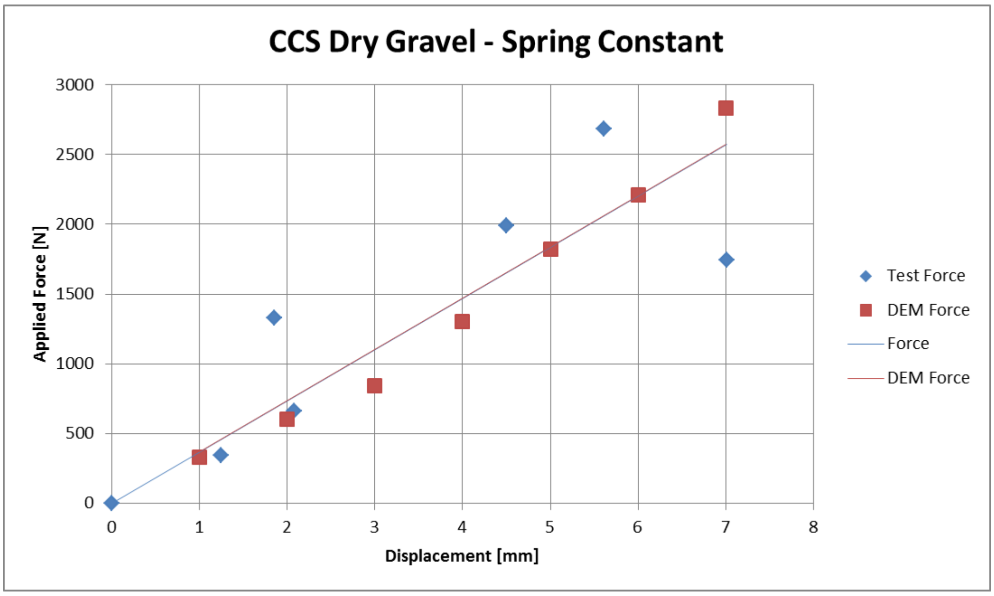

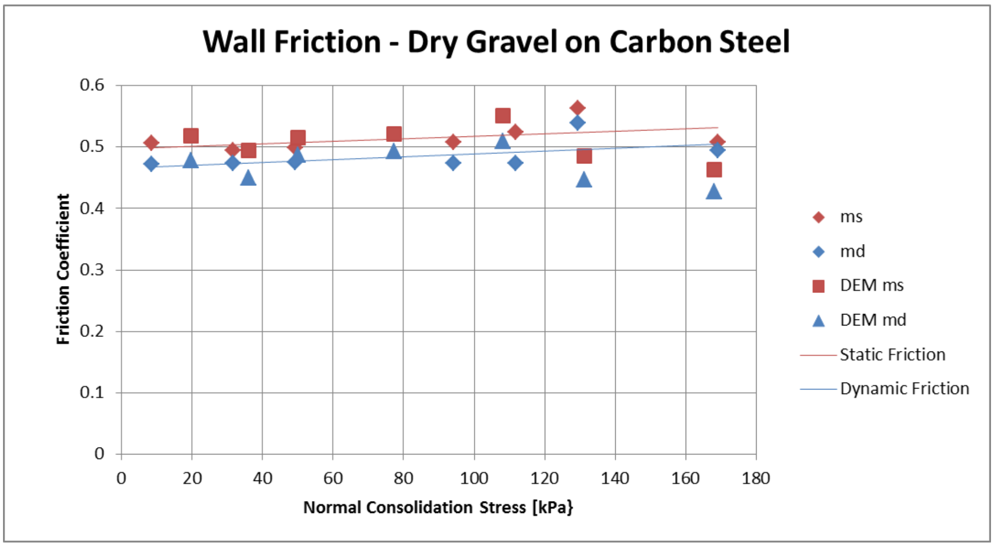

Particle stiffness	$3.6x10^7$ N/m^2
Wall friction – Static	0.67
Wall friction – Dynamic	0.65
Internal friction – Static	0.29
Internal friction - Dynamic	0.25
Cohesion factor	0.0
Adhesion factor	0.0

Figure 5-6. Spring andfFriction curves for dry gravel – wall friction.

5.6.2 Dry fines

Figures 5-7 and 5-8 show the final spring curves and friction curves for the dry fines (M3 material) wall and internal friction tests, respectively.

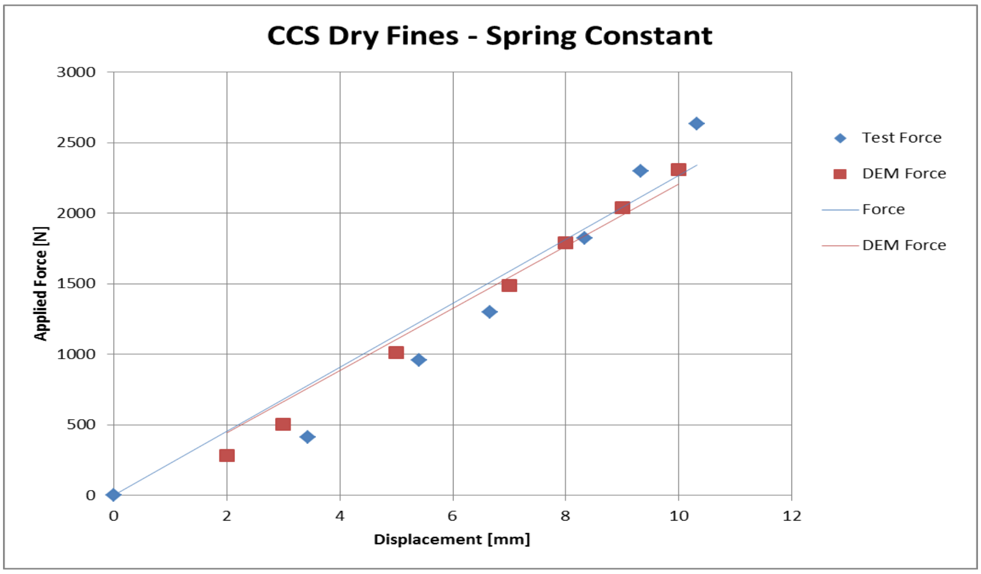

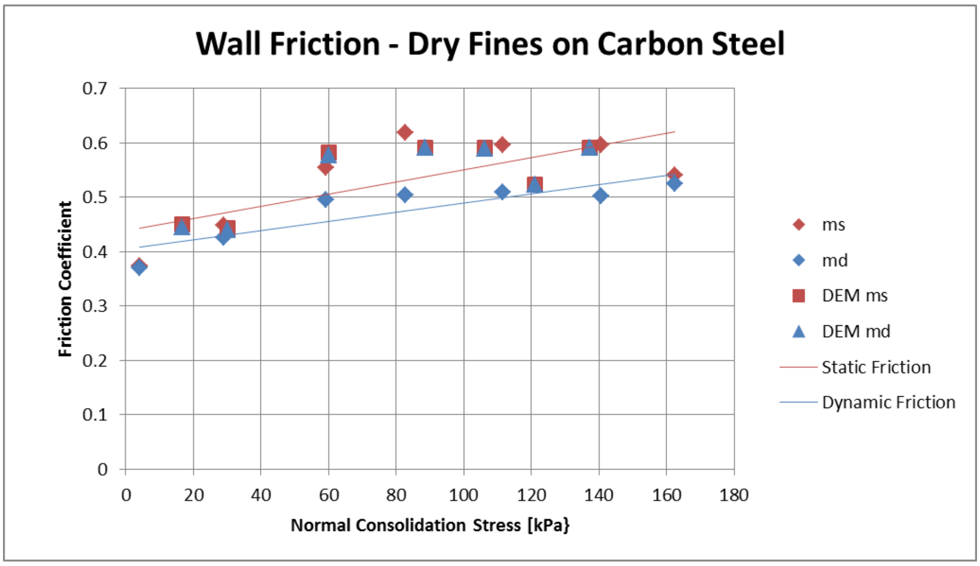

Particle stiffness	$8.0x10^6$ N/m^2
Wall friction – Static	0.5
Wall friction – Dynamic	0.5
Internal friction – Static	0.5
Internal friction - Dynamic	0.5
Cohesion factor	0.0
Adhesion factor	0.007

Figure 5-7. Spring and friction curves for dry fines – wall friction.

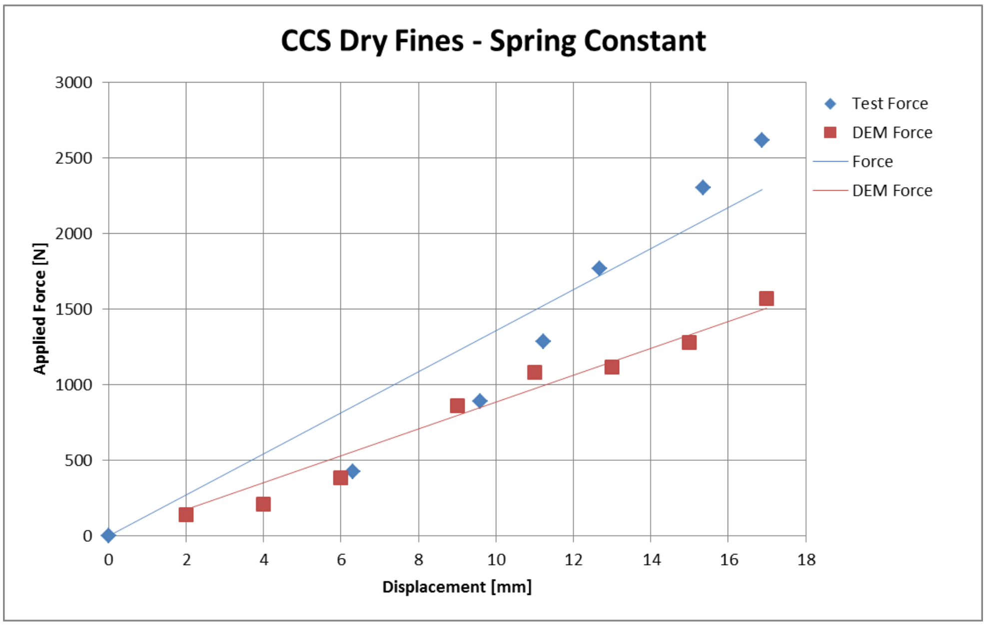

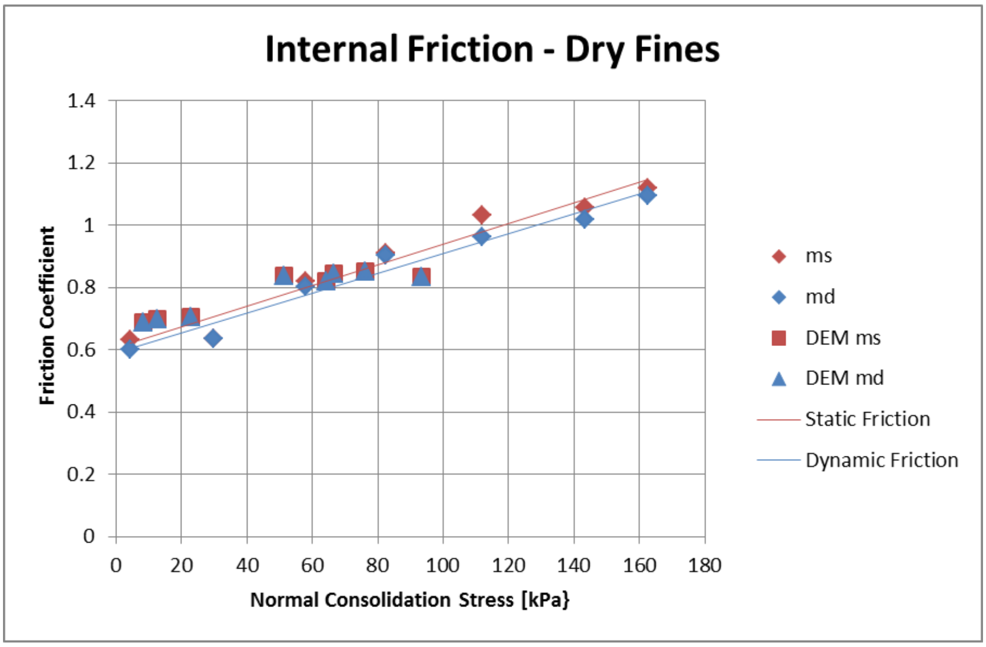

Particle stiffness	$8.0x10^6$ N/m^2
Wall friction – Static	0.5
Wall friction – Dynamic	0.5
Internal friction – Static	0.5
Internal friction - Dynamic	0.5
Cohesion factor	0.0
Adhesion factor	0.007

Figure 5-8. Spring and friction curves for dry fines – internal friction.

While the spring curve slope on the wall friction simulation is a 97% match to the test data, the internal friction spring curves only match to about 65%. This, along with the maximum consolidation stress of less than 100 kPa indicates that the stiffness needs to be increased.

Due to the positive slopes of the dry fines friction curves, a small adhesive force factor was added to the particles. Otherwise the simulations would have produced essentially constant flat lines with no increase in friction as the consolidation pressure was increased.

5.6.3 Wet Fines

The particle stiffness curve for the wet fines is dependent on the adhesive and cohesive force factors, as both of these factors alter the spring curves and the range of consolidation stress in the friction curves.

Iterations for this material began with the assumption that the stiffness of the individual particles is the same as that found for the dry fines, and that the difference in the stiffness curves for the bulk wet material are due to the cohesive and adhesive forces. This turned out to not be the case, and the stiffness that works best for the wet fines is considerably less than the optimum stiffness for the dry fines.

The simulation spring curves are a bit on the high side, with the wall friction spring curve at 121% of the test values and the internal friction spring curve at 142% of the test values. However, this was necessary to move the obvious plateau in the internal friction curve up the scale so that the linearly increasing portion of the curve covered a substantial part of the compressive stress range. A good fit on the friction curve is more important than a perfect fit on the spring curve.

It is worth mentioning that at the point where the internal friction curve flattens out, the force required to move the simulated test cell 10 mm exceeds the maximum tangential force programmed into the simulation, and the mobile test cell sticks to the stationary test cell, just as it did in the actual tests. The consolidation pressure that this occurs at in the simulation is between 99 kPa and 127 kPa, whereas in the test it occurred between 55 kPa and 86 kPa. This indicates that either the stiffness or the cohesive force factor are too high, and needs to be reduced. While this reduces the simulation's ability to match the test friction curve at higher consolidation pressures, the chute drop heights that correspond to these high consolidation stresses are in excess of 6 m.

Figures 5-9 and 5-10 show the final spring curves and friction curves for the wet fines (M3 material), wall and internal friction tests, respectively.

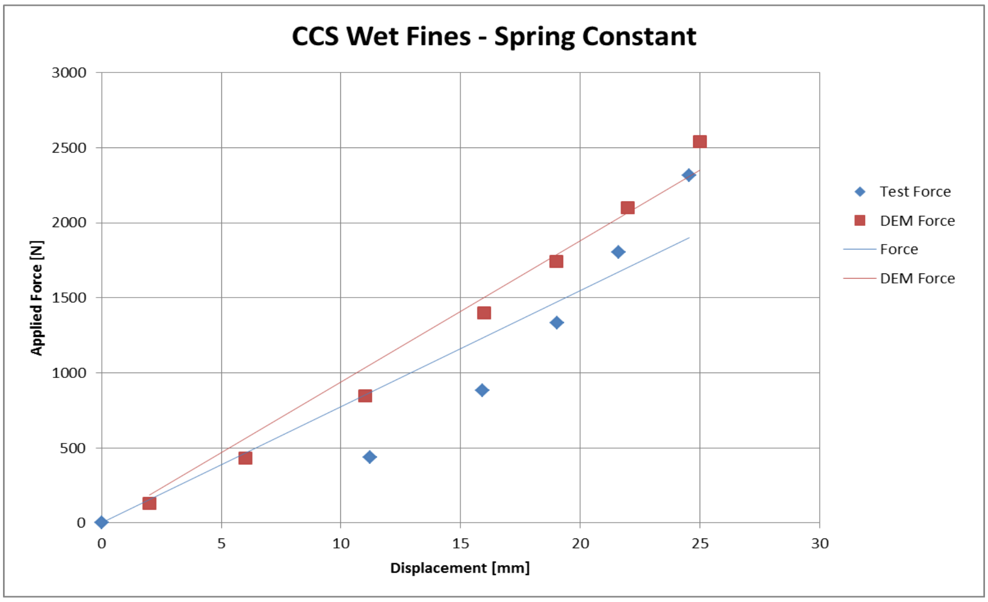

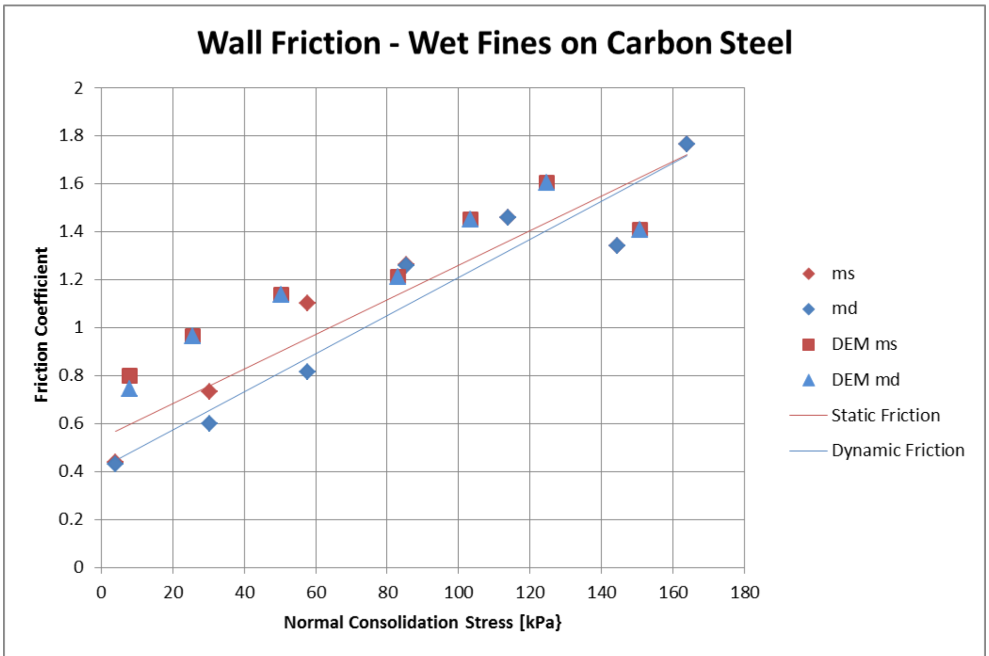

Particle stiffness	$8.0x10^6$ N/m^2
Wall friction – Static	0.5
Wall friction – Dynamic	0.5
Internal friction – Static	0.5
Internal friction - Dynamic	0.5
Cohesion factor	0.18
Adhesion factor	0.04

Figure 5-9. Spring and friction curves for wet fines – wall friction.

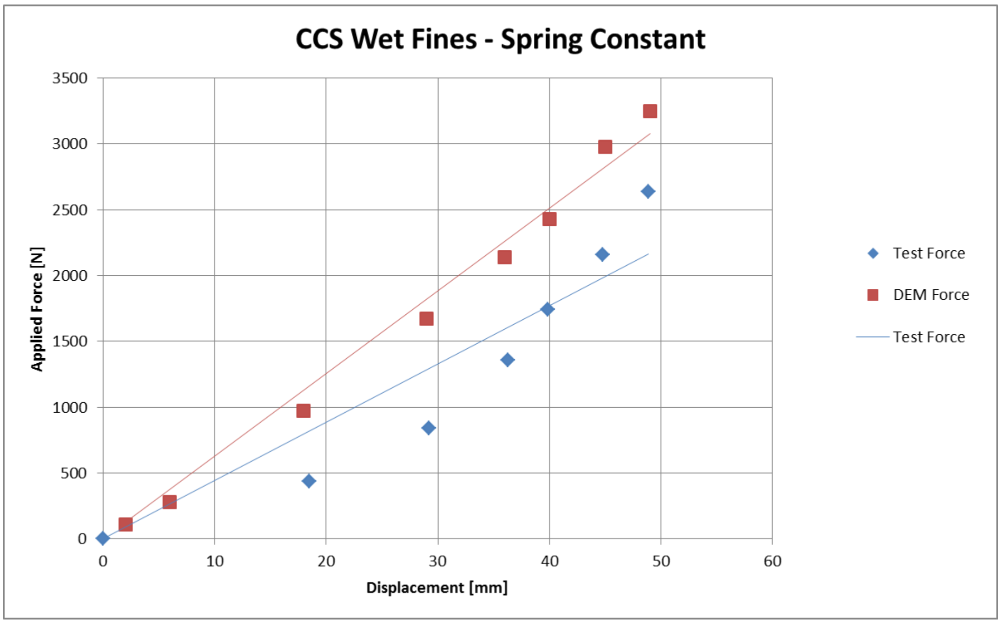

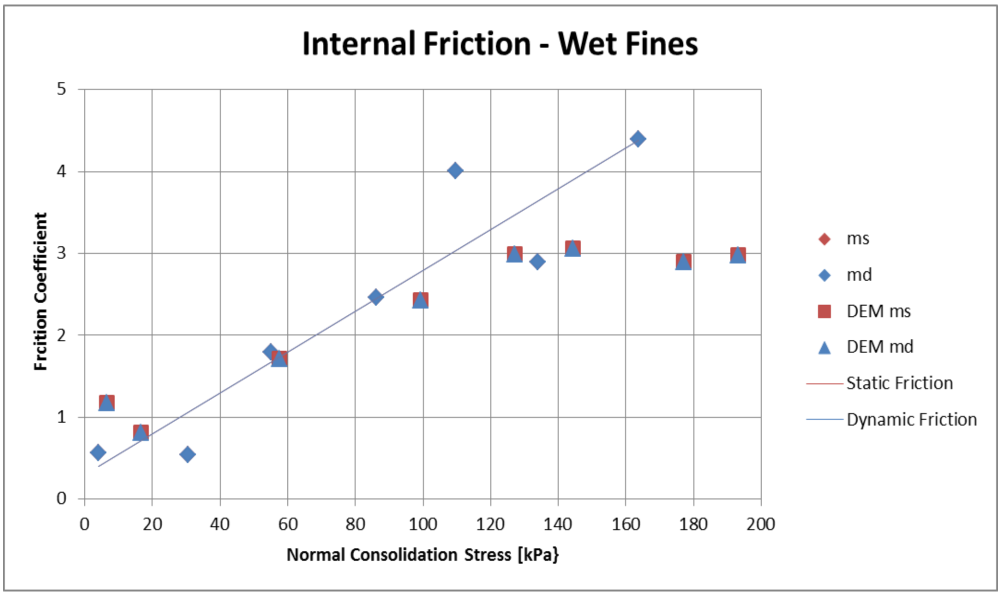

Particle stiffness	$8.0\text{x}10^6$ N/m^2
Wall friction – Static	0.5
Wall friction – Dynamic	0.5
Internal friction – Static	0.5
Internal friction - Dynamic	0.5
Cohesion factor	0.18
Adhesion factor	0.04

Figure 5-9. Spring and friction curves for wet fines – internal friction.

Table 5-5 summarises the final DEM particle stiffness's and friction factors developed for all four material types.

Material Type	Stiffness [N/m^2]	Wall Friction		Internal Friction	
		Static	Dynamic	Static	Dynamic
M1	6.0 x 10^6	0.50	0.47	0.81	0.79
M2	3.6 x 10^7	0.67	0.65	0.29	0.25
M3 - Dry	8.0 x 10^6	0.5	0.5	0.5	0.5
M3 - Wet	2.8 x 10^6	0.5	0.5	0.5	0.5

Table 5-5. Particle stiffness and friction.

6. ADHESION AND COHESION

Different DEM programs use different types of formulae to simulate the effects of adhesive and cohesive forces. The following discussion may not be strictly relevant to programs using different adhesion models.

ROCKY DEM can be set up to use one of two different cohesive/adhesive force factor models. The constant force model applies a constant force during the particle impact that is proportional to the mass of the particle. The linear force model applies a force that is proportional to the overlap distance computed during the impact cycle and the particle stiffness.

The constant force model adds an additional constant force to the normal force that the impact creates on the particle. Calculated friction coefficients using this model would result in a line similar to those produced with no cohesion or adhesion, but the line would be offset upwards. The slope would remain the same, but the magnitude at any given consolidation pressure would be higher.

The linear force model applies a force proportional to the material stiffness and the calculated overlap distance, or simulated particle deformation. This force increases more or less linearly as the consolidation pressure increases. This model allows for a linear approximation to the sloped curves observed in the test data for the dry and wet fines fractions.

Both of these models are labeled as 'adhesive model' in ROCKY DEM, and the way that the programmer differentiates between cohesive forces and adhesive forces is by specifying the material interactions between particles and like particles, or between one subset of particles and another subset, or between particles and boundary surface materials.

Both models include an input parameter called 'adhesive distance' which causes the force to begin to affect the particle motion at a distance greater than the actual particle radius. Because this parameter affects the particle diameter in the adhesive and cohesive force, it can have non-intuitive effects on the magnitude of the adhesive or cohesive forces calculated using the linear force model. Increasing the effective particle diameter reduces the amount of particle overlap, and the cohesive force decreases.

Because of this effect, and since the linear force model was needed to make it possible to match the test friction curves, this parameter was set to 0.0 for all calibration simulations.

Table 6-1 summarises the cohesive and adhesive force factors applied to the simulations performed on each particle fraction or material type.

Material Type	Cohesive Force Factor	Adhesive Force Factor
M1	0.0	0.0
M2	0.0	0.0
M3 – Dry	0.0	0.007
M3 - Wet	0.18	0.04

Table 6-1. Cohesive and adhesive force factors.

7. COEFFICIENT OF RESTITUTION

This parameter has a typical default value of 0.3, based on studies done on the rebound heights and velocities of typical hard rock ores. If all the fines as particles of the actual size distribution found in the bulk material could be modelled, this would probably be satisfactory. However, it is plain to the smallest child making sand castles and mud pies that a handful of sand, or a ball of mud, does not bounce the way a solid chunk of rock of equal mass would.

At this time, there is no satisfactory way of measuring this parameter in a real world test situation. The standard drop tests that work for 25 mm rocks won't work for a collection of very small particles with the same mass as the 25 mm rock.

Dry fines would dissipate and segregate due to atmospheric drag as they dropped, and it would be difficult to measure the average rebound height of millions of small particle impact events.

A 25 mm ball of wet fines, or dry fines in a loosely bound conglomerate, impacting at a given velocity would tend to lose more energy in deformation and fracturing than a rock would in similar circumstances, and would therefore bounce less.

To these problems of real world physics must be added a problem with stability of the DEM program's solver kernel. For instance, ROCKY DEM has a hard lower limit of 0.1 on this input parameter, as below that value the solver has difficulty in converging on trajectory solutions.

Until such time as a viable test method can be developed, the coefficient of restitution should remain at the recommended default value of 0.3.

8. CONCLUSION

This study shows it is possible to design a combination of material tests and DEM simulations that enable a set of 25 mm DEM particles to behave similarly to an equivalent mass of much smaller fine particles. As part of this process, it is essential to separate and measure the properties of the bulk material at several different scale levels:

- Particles that can be effectively simulated by the DEM program with no modifications to their material test results. These particles are represented by the M1 class: a subset consisting of particles in the size range from +25 mm up to the largest lump in the bulk material, modelled as non-round particles with the same size distribution as found in the bulk material.
- Particles which are smaller than the smallest particle included in the DEM particle set, but which are larger than the effective distance of liquid bridge, or other adhesive/cohesive forces. These particles are represented by the M2 class: particles in the size range from +6 mm to -25 mm modeled as 25 mm spheres.
- Particles which are so small that they are affected by adhesive/cohesive forces: These particles are represented by the M3 classes: particles in the -6 mm size range modeled as 25 mm spheres.

To make appropriate adjustments to the 25 mm DEM particles, it is necessary to adjust particle density, stiffness, and friction coefficients so that a bulk collection of 25 mm DEM particles generates the same resistance to compaction, and the same resistance to tangential forces, as a bulk collection of the +6 mm to -25 mm and -6 mm particles of equal total mass would have.

9. NEXT STEPS

This study is far from complete.

- A mixture of these three particle types with these specific input parameters has yet to be used in a chute design simulation.
- Several of the calibration iterations described here need additional iterations before the calibration can be completed. However, at this time these iterations would be of dubious value until a trajectory analysis of proposed chute design is performed so that a realistic maximum compressive stress limit can be set. Such a limit would reduce the number of iterations required to obtain a calibration that is well-suited to the design intent.
- Additional tests involving different levels of moisture content would be beneficial in developing a better understanding of how moisture affects the adhesive and cohesive properties of this particular material.
- A suitable test method for determining the coefficient of restitution of a handful of fines needs to be developed.

REFERENCES

1 Wensrich, C.M and Katterfeld, A. (2012). "Rolling Friction As a Technique for Modeling Particle Shape in DEM." *Powder Technology*, Vol. 217, pp. 409-417.

BIBLIOGRAPHY

1 Juan Ai, Jian-Fei Chen, J. Michael Rotter, Jin Y Ooi (2011). "Assessment of rolling resistance models in discrete element simulations", *Powder Technology*, Vol. 206. pp. 269-282, 2011.

2 Dawei Zhao, Erfan G. Nezami, Youseef M.A. Hasash and Jamshid Ghaboussi (2006). "Three-dimension discrete element simulations for granular materials", *Engineering Computations: International Journal for Computer-Aided Engineering and Software*, Vol. 23, No. 7, pp.749-770.

3 Ludig, Stefan (2008)."Cohesive, frictional powders: contact models for tension", *Granular Matter*, Vol. 10, pp. 235-246.

4 Bushan, Bharat (2003) "Adhesion and stiction: Mechanisms, measurement techniques, and methods for reduction." *J. Vac. Sci. Techol. B*, Vol. 21, No. 6.

5 Johanson, J.R. (1992). "The Johanson Indicizer System vs. the Jenike Shear Tester." *Bulk Solids Handling*, Vol. 12, No. 2.

6 Horn, Etienne (2102) "The Calibration of Material Properties for Use in Discrete Element Models." *Masters Thesis*, Dept. of Mechanical and Mechatronic Engineering, Univ. of Stellenbosch.

7 Jenike, A.W. (1964). "Storage and flow of solids, Bull. No. 123", Engng. Exp. Station, Univ. Utah, Salt Lake City.

8 CEMA Standard 550 (2009) "Classification and Definitions of Bulk Materials", ANSI/CEMA 550-2003-R2009.

9 Coetzee, C.J. (2016). "Calibration of the discrete element method and the effect of particle shape." *Powder Technology*, Vol. 297, pp.50-70.

10 Wancheck, G.A. and Fowkes, R.S. (1973). "Materials Handling Research: Shear Properties of Several Granular Materials." U.S. Dept. of Interior, Bureau of Mines, Report of Investigations 7731.

11 Gröger, Torsten and Katterfeld, André (2006). "On the Numerical Calibration of Discrete Element Models for the Simulation of Bulk Solids." *16th European Symposium on Computer Aided Process Engineering and 9th International Symposium on Process Systems Engineering*, pp. 533-538.

12 Yu Qian, Seung Jae Lee, Erol Tutumuer, Youssef M.A. Hasash, Debakanta Mishra, and Jamshid Ghaboussi (2013). "Discrete Element Method for Simulating Ballast Shear Strength form Large Scale Triaxial Tests." *92nd Annual Meeting of the Transportation Research Board*, Washington, D.C.

ABOUT THE AUTHOR

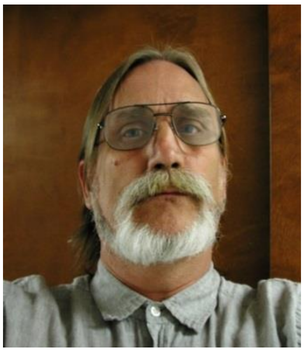

MICHAEL E. THOMPSON, P.E.

M.S. Mech. Eng. - The Ohio State University (1997)
Ohio P.E. License (2003)
Washington P.E. License (2009)
Senior Engineer at Conveyor Dynamics, Inc.
Eight years conveyor design experience.
Lead Design Engineer for 27 km Impumeleo OLC.
Five years DEM chute modelling experience.

Michael E. Thompson
3633 Alderwood Ave.
Bellingham, WA 98225
(360) 671-2200
thompson@conveyor-dynamics.com